NASA TECHNICAL NOTE

NASA TN D-7187

NASA TN D-7187

PERFORMANCE OF AN ION-CYCLOTRON-WAVE PLASMA APPARATUS OPERATED IN THE RADIOFREQUENCY-SUSTAINED MODE

by Clyde C. Swett and Richard R. Woollett

Lewis Research Center
Cleveland, Ohio 44135

NATIONAL AERONAUTICS AND SPACE ADMINISTRATION • WASHINGTON, D. C. • MARCH 1973

1. Report No.	2. Government Accession No.	3. Recipient's Catalog No.
NASA TN D-7187		

4. Title and Subtitle	5. Report Date
PERFORMANCE OF AN ION-CYCLOTRON-WAVE PLASMA APPARATUS OPERATED IN THE RADIOFREQUENCY-SUSTAINED MODE	March 1973
	6. Performing Organization Code

7. Author(s)	8. Performing Organization Report No.
Clyde C. Swett and Richard R. Woollett	E-7213
	10. Work Unit No. 503-10

9. Performing Organization Name and Address	11. Contract or Grant No.
Lewis Research Center National Aeronautics and Space Administration Cleveland, Ohio 44135	
	13. Type of Report and Period Covered
12. Sponsoring Agency Name and Address	Technical Note
National Aeronautics and Space Administration Washington, D.C. 20546	14. Sponsoring Agency Code

15. Supplementary Notes

16. Abstract

An experimental study has been made of an ion-cyclotron-wave apparatus operated in the rf-sustained mode, that is, a mode in which the Stix rf coil both propagates the waves and maintains the plasma. Problems associated with this method of operation are presented. Some factors that are important to the coupling of rf power are noted. In general, the wave-propagation and wave-damping data agree with theory. Some irregularities in wave fields are observed. Maximum ion temperature is 870 eV at a density of 5×10^{12} cm^{-3} and rf power of 90 kW. Coupling efficiency is 70 percent.

17. Key Words (Suggested by Author(s))	18. Distribution Statement
Plasma radiofrequency heating; Plasma waves; Plasma temperature; Plasma losses; Plasma composition; Magnetohydrodynamics; Controlled fusion; Plasma diagnostics; Plasma density; Plasma spectra; Plasma decay; Magnetohydrodynamic waves	Unclassified - unlimited

19. Security Classif. (of this report)	20. Security Classif. (of this page)	21. No. of Pages	22. Price*
Unclassified	Unclassified	43	$3.00

* For sale by the National Technical Information Service, Springfield, Virginia 22151

PERFORMANCE OF AN ION-CYCLOTRON-WAVE PLASMA APPARATUS OPERATED IN THE RADIOFREQUENCY-SUSTAINED MODE

by Clyde C. Swett and Richard R. Woollett

Lewis Research Center

SUMMARY

An experimental study has been made of an ion-cyclotron-wave apparatus operated in the radiofrequency-sustained mode, that is, a mode in which the Stix radiofrequency (rf) coil both propagates the wave and maintains the plasma for periods of 10 seconds to a few minutes. Apparatus and instrumentation problems associated with this method of operation are presented. Some factors that are important to the coupling of rf power to the plasma are noted. The operating range of the present equipment appears to be limited to transmitter power less than 120 kilowatts because of the heat load on the aluminum oxide center section and because of rf breakdown voltage problems. In general, the wave-propagation and wave-damping data agree with theory. Some irregularities in wave fields are noted. The maximum ion temperature measured in the magnetic beach is about 870 electron volts at a density of 5×10^{12} ions per cubic centimeter and a transmitter rf power of 90 kilowatts. The coupling efficiency, or the ratio of power in plasma to the transmitter output power, is 70 percent.

INTRODUCTION

Many theoretical and experimental investigations of ion cyclotron waves in plasmas have been conducted because such waves can be used by means of a thermalization process in a magnetic beach to heat plasma ions to extermely high temperatures. Stix (ref. 1) was the first to show the existence of oscillations near the ion cyclotron frequency, and Stix and Palladino (ref. 2) experimentally showed resonant power absorption near the ion cyclotron frequency. Subsequently, many investigators have observed resonant power absorption, have identified the propagating ion cyclotron wave, and have shown damping in a magnetic beach with resulting high ion temperatures. Hooke and

Rothman (ref. 3) have summarized most of the ion wave experiments prior to 1963 in a bibliography. Some later theoretical and experimental investigations are reported in references 4 to 23.

The experimental procedure most widely used in these investigations has been to create a plasma and then apply a pulse of high-frequency current to a Stix radiofrequency (rf) coil to generate the waves. Studies of wave propagation and wave damping are conducted during or after the pulse.

An exception to this procedure is found in the experiments at the NASA Lewis Research Center where the ion cyclotron wave phenomenon was studied in a steady-state system. In early experiments (refs. 4 to 8, 11, and 12), the plasma was generated by a hot-cathode arc discharge, and a steady-state rf current was applied to the rf coil. Waves in the plasma were then studied for periods up to about 10 minutes.

These steady-state experiments require cooling the equipment and instrumentation, and thus lack the high power capability of the pulse experiments. However, they do have several advantages. Since complete wave measurements can be recorded within a few seconds, the problem of variations in reproducibility that may overshadow fine structure is avoided. A perfect match between the rf transmitter and the Stix coil can be attained. Direct heat-balance measurements can be obtained for studying losses from the plasma. Also, a steady-state high-temperature is desirable for many fundamental studies.

Results by Swett, Krawec, and Hettel (ref. 6) show that as the rf power is increased the hot-cathode arc discharge becomes unimportant and can be turned off, whereupon the plasma is sustained by the rf. This method of operation (the rf-sustained mode) has been used in more recent studies of ion cyclotron waves.

As the investigation evolved, a number of techniques were developed to surmount certain operating and instrumentation problems. Also studied were some features of the apparatus that appeared important to the coupling of rf power to the plasma. The present report discusses the performance of the apparatus and includes sufficient data on ion cyclotron waves so that results can be compared to those obtained with pulse systems.

SYMBOLS

B magnetic field at diamagnetic coil, T

$\dot{B}_r$ time derivative of radial magnetic component of wave, T/sec

$\dot{B}_z$ time derivative of axial magnetic component of wave, T/sec

$\dot{B}_\theta$ time derivative of azimuthal magnetic component of wave, T/sec

E	radial electric field, V/cm
e_0	output voltage of diamagnetic coil, v
M	magnetic moment, $4\pi\times10^{-7}\ \pi r_p^2$
N	number of turns on diamagnetic coil
n_e	electron density, cm^{-3}
r_p	plasma radius, cm
RC	time constant of integrator, sec
T_e	electron temperature, eV
T_i	ion temperature, eV
λ	wavelength, cm
Ω	frequency ratio

EXPERIMENTAL EQUIPMENT

The basic features of the apparatus used are shown in figures 1 to 5. Briefly, the apparatus consisted of a long cylindrical vacuum tube surrounded by magnetic field coils and an rf coil. In the presence of hydrogen (H_2) or deuterium (D_2) plasma and the proper magnetic field, the rf coil induced ion cyclotron waves which propagated toward two magnetic beach regions. A hot-cathode arc discharge throughout the length of the system produced the plasma to which the rf power was coupled. Grid structures located near the peak magnetic field of the mirror coils were essential parts of the system. The apparatus as a whole was designed for steady-state (greater than 10 sec) operation.

Magnetic Field and Control

The magnetic field was of the mirror type with a flat-field region between the mirrors. The uniformity of this flat-field region was approximately ±1 percent. The current for the coils was supplied by two dc generators, the fields of which were energized by a selenium-controlled-rectifier power supply. This power supply in turn was controlled by a signal from a rotating coil gaussmeter imbedded in a coil separator near the center of the system. Control of the magnetic field by this method was approximately $\pm3\times10^{-5}$ tesla. The field intensity could also be swept from minimum to maximum at any desired rate.

Either of two magnetic beaches (ref. 2), designated as near beach and far beach, could be used for wave damping experiments. Because the wave damps quickly, only results using the near beach are reported herein. A separate variable power supply connected to the near-beach coils permitted the magnetic beach to be varied between the limits shown (0 to 12 percent).

Vacuum Chambers

Two different types of stainless-steel arms were attached to the rf section to form part of the vacuum chamber. Type I had a 10-centimeter inside diameter with double walls between which a measured amount of water flowed axially for cooling. This type is shown in figure 1. Thermocouples were located every 2.5 centimeters along the tubes in the water passage for heat-balance measurements. Type II had a 13-centimeter inside diameter, was single-walled, and had tubing welded on the exterior surface for water cooling. This latter type also had flanges for installation of the grid structures at the position of maximum field in the mirror. For the type I installation it was necessary to mount the grid structures at the outermost window position which was not quite at the maximum field position.

Rf Section

The outer shell of the rf section (fig. 2) was stainless steel; its inner surface had been silver plated and gold flashed to reduce eddy-current heating losses. The rf coil was a four-section Stix coil having four turns per section. The coil inside diameter was 14.2 centimeters and the wavelength distance between the center of the first section and the center of the third section was 41.0 centimeters. It was fabricated from 0.95-centimeter diameter stainless-steel tubing because of its structural rigidity, was plated as described previously and was water cooled.

Inside the rf coil were two concentric alumina cylinders between which a silicone oil flowed for cooling. Oil flow rates and temperatures were measured to determine the heat transfer from the plasma to the alumina test section. The inner diameter of the innermost cylinder was 8.9 centimeters; the wall thickness of the cylinders was 0.64 centimeter.

An electrostatic shield was located in the oil passage between the alumina cylinders. It consisted of 25 unplated copper strips 1.27 centimeter wide by 0.079 centimeter thick and spaced 0.16 centimeter apart. The strips were grounded at both ends to the outer shell by means of radial plates so that the rf coil was completely enclosed by high con-

ductivity surfaces. The coil-shield combination had a Q of 433 at 6.5 megahertz with no plasma load. The coil inductance as measured at the coaxial rf feed (fig. 2) was 2.5 microhenry; the coil resistance was 0.254 ohm.

For the oxygen elimination test, a water-cooled stainless-steel shield (fig. 6) was placed inside the innermost alumina cylinder to prevent direct bombardment of the cylinder by the plasma.

Rf System and Control

The rf power source used to drive the Stix coil was either a 45- or 150-kilowatt transmitter operated at 6.5 megahertz. The 600-ohm balanced output of the 45-kilowatt transmitter was matched to a 50-ohm coaxial line by means of a balun transformer. The 150-kilowatt transmitter was constructed with a 50-ohm output. A 50-ohm L-type matching network was used to complete the matching to the rf coil. The matching network is described in reference 12. A control system on the transmitter was used to maintain the rf coil current constant at any predetermined value regardless of load. Another automatic control system operated the two motor-driven vacuum capacitors in the matching network so that the transmitter was always operated with a 50-ohm load, which eliminated power losses and excessive voltages due to reflections. Such control was necessary when sweeping the magnetic field for resonant power-absorption measurements. It was a powerful aid during plasma startup, and it also simplified the required adjustment of two capacitors as the plasma loading gradually changed with time.

Initial Plasma Source

The initial source of plasma was a hot-cathode discharge produced by a squirrel-cage arrangement of 18 heated spiralled-tungsten wires (fig. 5) operated at a potential which was negative with respect to the metal vacuum chamber. The plasma column was intercepted by grid structures (fig. 3) located at or near the peak field of each mirror. These structures were connected electrically as shown in figure 4. When voltage was applied to the hot cathode, a discharge (currents up to 80 A) was established. Because of the resulting voltage drop across the resistor, the discharge passed through the first grid and continued to the second grid. When the plasma was maintained by the rf power the tungsten strips composing the grids had a temperature of 1900 to 2000 K as indicated by an optical pyrometer. Because of the heat conduction along the strips, the straight grids were heated in a wide band, whereas with the circular grid, the hot

area was circular because of reduced heat conduction. The latter type was preferred both from the fabrication standpoint and slightly improved performance.

INSTRUMENTATION

Power-, Current-, and Voltage-Measurement Systems

Power to the rf coil was measured by means of a directional coupler located in the 50-ohm transmission line. Separate forward and reverse power meters were located in the control room. These meters were calibrated using a 50-ohm calorimeter having an accuracy of ±1 percent.

Current was measured by a current transformer placed in series with the rf coil. A vacuum tube voltmeter measured the coil voltage. The transformer and voltmeter were located in the matching network box with provision for readout in the control room.

Rf Magnetic-Probe Systems

Three different systems were used in local rf magnetic probing of the plasma: (1) a hydraulic-piston-actuated radial traverse (fig. 7(c)) from one wall to the center of plasma at the two window positions (fig. 1), (2) and arc traverse (fig. 7(c)) through the plasma at any axial position desired, and (3) an axial traverse with the probe placed at or near the center of the plasma. The latter two traverses were accomplished manually. In these two measurements the probe coils were in water-cooled quartz tubes. Because the radial traversing probe was in the plasma only momentarily, the probe coil was in an uncooled Vycor glass tube.

Probe coils used throughout the investigation were 10-, 20-, or 40-turn two-layer coils having an inside diameter of 0.13 centimeter. The coils were calibrated in a Helmholtz coil using a method somewhat similar to that described in reference 24. The actual circuit used is shown in figure 7(d).

Some measurements were made of all three magnetic components of the wave, $\dot{B}_z$, $\dot{B}_r$, and $\dot{B}_\theta$. In the radial traversing system, the measurement of all three components was straightforward. In the arc traversing system, $\dot{B}_z$ was the only component that could be measured without applying a correction factor. In the measurement of $\dot{B}_r$ and $\dot{B}_\theta$ there is a slight mixing of components. The amount of mixing varies from 0 to a maximum of 6 percent depending on the probe position as it sweeps across the plasma. This effect is considered when discussing the results.

The measurement of the probe output voltages and phases with respect to the Stix rf coil voltages was accomplished by the circuitry shown in figure 7(e). The Stix coil voltage was reduced and applied to a phase shifter or delay line so that the initial phase difference could be set to zero or any other value desired. The phase difference between probe voltage and Stix coil voltage was then measured either by the oscilloscope or the Hewlett-Packard 8405A Vector Voltmeter. This instrument reads out directly both phase and amplitude; it also had phase and amplitude outputs suitable for X-Y plotters. Hence, as the probe was moved, the changes in phase and amplitude were plotted directly as a function of position. The wavelength of the plasma wave was determined from the phase change over measured distances.

Total $\dot{B}_z$ Probe

The total axial magnetic flux of the propagating wave was measured by means of a single loop of wire wrapped around the plasma (fig. 8). This loop was encased in a stainless-steel tube having an opening so that the magnetic field was not shielded out. The tube was water cooled and could be moved axially.

The output of the loop was connected to a differential amplifier which in turn was connected to the equipment used with the magnetic-probe system. Hence, as the total $\dot{B}_z$ probe was moved, the phase and amplitude of the signal were recorded on X-Y plotters. These recordings gave another measurement of the plasma wavelength.

Diamagnetic Coil System

Transverse ion temperature measurements were made by means of 100-turn coils wound on the vacuum chamber arms in the vicinity of the magnetic beach. These coils measured the plasma diamagnetism when the rf transmitter was unkeyed.

Instrumentation for the diamagnetic coils is shown in figure 9. The techniques used were developed using reference 25 as a guide. The circuit provided compensation for wall eddy currents so that the rate of temperature change could be determined.

At low ion temperatures it was necessary to reduce noise pickup from the dc magnetic system. The best method for doing this was by means of a bucking coil that sensed the fluctuations in the magnetic field. A certain amount of the signal was subtracted from that of the diamagnetic coil in a summing circuit. For most of the higher ion temperatures (as reported herein), it was not required that the bucking coil be used.

The sum of the ion and electron temperatures (T_i, T_e) in the perpendicular direction is given by

$$T_i + T_e = \frac{6.25\times10^{16}\, B(RC)e_0}{NMn_e}\ eV$$

where

B magnetic field at diamagnetic coil, T

RC time constant of integrator, sec

e_0 output of circuit, V

N number of turns of coil

M magnetic moment, $4\pi\times10^{-7}\left(\pi r_p^2\right)$, cm

r_p plasma radius, cm

n_e electron density, cm^{-3}

This equation can be derived from equations in reference 25. As is shown later, since the electron temperature was negligible when compared with the ion temperature, $T_e = 0$ was used in the calculations. No correction was made for the finite resolution of the coil. However, as shown in reference 18, the error in the measurement of T_i in a beach region where the transverse temperature is changing rapidly with axial distance is no more than 20 percent low.

Langmuir Probe System

A Langmuir probe was used to measure electron temperature and ion density in plasmas. This probe was driven through the plasma and back by a hydraulically operated piston from a wall recess. An electronically controlled valve varied the speed at which the probe moved through the plasma. The probe could be stopped at any position and could be held there for any length of time. During this dwell time, the probe voltage was swept to give a Langmuir trace on an oscilloscope. Dwell times were typically 0.1 second, voltage-sweep times were 0.05 second, and total travel time (in and out) was 0.1 second.

Each probe was a quartz-covered tungsten wire with an exposed length of 0.254 centimeter (0.1 in.). The wire was 0.0508 centimeter (0.020 in.) in diameter. The traces were analyzed for electron temperature, and the ion density was determined by the method described by Krawec (ref. 26).

Spectrometers

Two spectrometers were used: (1) a 1.5-meter two-mirror spectrograph (Jarrell-Ash model 75-100) and (2) a 0.5-meter EBERT scanning spectrometer (Jarrell-Ash moedl 82-100). The former was used primarily to study contamination and species present; the latter is being used to develop techniques to study line broadening for ion temperature measurements.

Neutral Particle Analyzer

A magnetic electron multiplier of the type described in reference 27 was used in conjunction with an energy analyzer to study the charge exchange neutrals coming from the beach region.

Neutron Flux Measurement

The neutron flux at the magnetic beach was measured by means of a portable neutron survey meter of the boron trifluoride (BF_3) type. The meter was modified by installing a counter on the output for single event counting.

EQUIPMENT PERFORMANCE AND LIMITATIONS

Perfromance of rf Section

The most critical area of the whole apparatus was the rf section because this section had the greatest heat load per unit area and had the high rf voltages. The critical elements were the two concentric aluminum oxide tubes located inside the rf coil. These tubes were required to withstand great heat load (inner tube) or high voltage (outer tube).

With a design heat load factor of about 7 watts per square centimeter the inner tube was expected to handle about 20 kilowatts. With measured power loss in the rf coil and with experimental facts on plasma heat loss to the tube, the present design should handle about 45 kilowatts total power continuously. Actually, some fracturing of the tubes was encountered in running at this power for time periods of 3 to 10 minutes. The fractures were mostly at the ends of the tube and appeared to be the result of thermal gradients there. Figure 10 shows a detail of the end region. The area where the tube

is chamfered appears to be inadequately cooled and was probably subject to thermal stresses that resulted in cracking.

Three improvements have been made in this design that have increased the service life: (1) the chamfered portion was shortened as much as possible to reduce the uncooled length, (2) the cooling oil was channeled better to eliminate any dead spots at the end regions, and (3) the limiter diameter was reduced to eliminate all possibility of axial plasma bombardment of the ends of the tube.

Since these changes were made, only one failure occurred at 45 kilowatts. However, when the capability was increased to 150 kilowatts, running time was limited to 1 minute for power up to 45 kilowatts and 10 seconds for power above 45 kilowatts with at least 1 minute between runs. An axial seal at the ends of the alumina tube would eliminate the uneven heating and cooling of the tube and allow longer running times.

A minor problem was encountered with the limiter rings. As the power was increased above 45 kilowatts, the limiter rings became overheated as indicated by molten spots and radial cracking. Eventually, the limiter rings were replaced with water-cooled tubes bent to fit on the inside circumference of the limiter spoolpiece.

High voltage (up to 60 kV peak) was no major problem. Only two tubes fractured at the point of greatest electric field - the center of the system. These failures were believed to be caused by improper machining that reduced the wall thickness to one-half the specified value. Problems are anticipated in the matching network at rf power levels approaching 150 kilowatts where about 60 kilovolts will be applied to a network capacitor rated at 55 kilovolts. Such problems can be solved by a series connection of two capacitors.

Performance of Instrumentation

Probes that are immersed in the rf sustained plasma (density, $\sim 5\times10^{12}$ cm^{-3}; ion temperature, 500 to 1000 eV; and electron temperature, ~15 eV) must either be adequately cooled or allowed to remain in the plasma only momentarily. The magnetic probe, total $\dot{B}_z$ probe, and Langmuir probe were immersed. The magnetic probe was in the plasma for long times (a few seconds at least); hence, it had to be well cooled. Some conditioning in the plasma was required because of the quartz tube surrounding this probe. It is believed that when this tube was heated to seal the end the resulting seal was too thick to allow good heat transfer between the plasma and water. The glass surface heated and eroded rapidly until some equilibrium thickness was reached. Thereafter, the probe had small effect on the plasma, at least at total rf power up to 35 kilowatts. At higher power the probe began to affect the plasma, as observed by reduced plasma loading.

The total $\dot{B}_z$ probe was not in direct contact with the plasma so that it had a negligible effect on power loading. Considerable energy did reach the probe by means of hot neutrals as evidenced by cooling-water temperature rise.

Successful use of the Langmuir probe depended on minimal residence time in the plasma. The object was to avoid heating the probe tip to electron emitting temperatures. The criterion used for determining this time was that ion saturation current measured as a function of position as the probe was going into the plasma had to be the same as that coming out. By trial and error, the total allowable travel time was found to be approximately 0.1 second or less.

Effect of Grids on Power Coupling

The grids were found to be necessary for operating in the rf-sustained mode. Originally, the system was operated without grids using only the arc discharge as the plasma source. Because of the construction of the filament structure and because electrons follow magnetic-field lines, the arc discharge was very striated. An attempt to break up the striations by introducting grid structures in nonsustained operation was unsuccessful, but improvement in rf power absorption was striking.

Figure 11 shows how the rf power absorption increased and how the maximum power point shifted for different operating modes. A shift toward greater magnetic fields implies an increased ion density. With a 50-ampere arc discharge (fig. 11(a)) the resonance is sharp with Ω very close to unity (Ω is the ratio of operating frequency to ion cyclotron frequency). Over a very narrow magnetic field range (shown by the 4 points in fig. 11(b)) the arc discharge could be turned off, the plasma being sustained by the rf only. This range occurred at smaller values of Ω than were measured when operating with an arc discharge and no grids. Since in addition power absorption increased, the indications were that the ion density had increased. When the grids for the type I arm were used, power absorption again improved and a further shift in Ω and in the operating range was noted (fig. 11(c)). These type I grids were slightly smaller than the plasma at window position. The straight grid for the type II arm (properly located at the peak of the mirror field and of size greater than the plasma diameter) again improved performance (fig. 11(c)). Subsequently, the circular grid for type II arm was constructed. This grid gave somewhat better performance than the straight grid and was easier to fabricate.

Inconsistencies in the position of the power loading peaks were encountered occasionally when grids were changed. It was found that slight tilting of the grid mount was necessary to achieve best power loading. Figure 12 shows the effect of tilting the grid about 10° from the vertical. Since the position of the peak power point is a measure of

density, tilting the grid has increased the density. Increasing the angle beyond this value offered no improvement in density. Supporting the grid in a manner to increase heat insulation also improved performance slightly. The density distribution, however, was improved by more tilting. The most uniform distribution was found with extreme tilting of 25^{o}, which is an angle such that an observer looking axially along the system cannot see through the grid.

Tilting the grid allowed more of the plasma to be intercepted. Visually the grid became noticeably hotter and the heating pattern more uniform. All of the experience with grids indicated that the temperature of the grid appeared to be correlated with rf coupling.

A number of experiments were conducted in an attempt to understand the mechanism whereby the grid controls the plasma. Electrical connections to the grid are unimportant for once the plasma is rf sustained, the grids could be electrically floated, grounded, or biased, with no effect on power coupling, wave propagation, or extinguishing of plasma. Probes or rods inserted in the plasma cast shadows in the direction away from the center of the system indicating that the plasma was being generated at the rf coil. The grid effect existed with and without a beach, which indicates that wave reflections at the grid need not be considered since the beach damped the wave before the grid was reached. The one explanation that appears to agree with all the facts observed and which appears to be the most likely is that the grid acted as a source for hydrogen atoms (ref. 28). The atoms could travel to the rf coil where ionization by electrons could occur. The axial electric fields under the coil were strong enough to ionize the atoms. (In fact, the fields were strong enough to dissociate and ionize molecules but the lower ionization potential of the atoms should make for easier ionization.)

The only evidence of the presence of atomic hydrogen was found in a spectrographic test. This test showed that the intensity of the excited atomic deuterium line was much greater near the grid than further away. This fact indicated that the grid was dissociating the molecular deuterium.

For atoms in excited states ionization is greatly increased (ref. 29). The grids might also have aided in producing such excited states.

System Conditioning

The system required a certain amount of plasma conditioning if it had been exposed to the atmosphere. On startup, a small amount of rf power was coupled to the arc discharge and a number of 30-second runs had to be made before the power absorption suddenly increased. Then the discharge could be turned off, the plasma being maintained by the rf. The number of runs required generally was about one to ten at coil

currents that would give 45 kilowatts under normal operating conditions. At low power (less than 15 kW) and without grids, it was not unusual to make more than 50 runs to complete the conditioning.

Once the system was rf sustained, it was found that about three runs would be required before maximum energy density (as measured by diamagnetic coils) would be attained in the beach. Apparently the strong bombardment of the wall in the beach region and elsewhere did some further conditioning.

If the system was maintained at low pressure, no conditioning was required to make the system rf sustained even days later.

Plasma Produced by rf-Sustained Mode

The plasma density, as previously indicated, was strongly dependent on the grids. Figure 13 shows a series of ion-density profiles taken with Langmuir probes at the beach position with varying amount of beach. As the beach was inserted, the plasma eventually became hollow and had a nonsymmetrical appearance. This is the type of data obtained when the grid is not tilted enough.

When the grid was sufficiently tilted, the profile with full beach became reasonably symmetrical (fig. 14). At higher power, the no-beach profile became more hollow and similar to the full-beach profile.

The amount of beach had no effect on the density at the bottom of the beach as shown in figure 15. The density ahead of the beach was slightly greater than that at the bottom of the beach. The density obtained at the usual operating condition (i.e., magnetic fields that give maximum ion temperature) was within the range of 3×10^{12} to 7×10^{12} ions per cubic centimeter for power from 45 to 100 kilowatts. Throughout this range, the average electron temperature was 11 to 17 electron volts.

Spectroscopic studies were undertaken to study the contamination of the plasma. Some observations and conclusions have been made. The percentage of oxygen impurity (from alumina tube) was determined to be about 8 percent during the first minute of a run. After 3 minutes, the oxygen percentage was 16 percent and still increasing. All of the major oxygen lines increased with time. Most of the spectrum was made up of oxygen and aluminum impurity lines; the intensity of the lines of both the elements increased or decreased simultaneously depending on operating conditions. Obviously, this contamination is from plasma bombardment of the alumina cylinder.

Spectra were also taken of iron and chromium (main constituents of stainless steel) lines at various positions along the axis. The intensity of these lines was greatest at the beach port window when a beach was present. At windows on either side of the beach, the intensity of the lines was greatly attenuated. When the beach was removed,

the intensity of the lines was sharply reduced. These results indicate that a high energy plasma-wall interaction was taking place at the beach.

An attempt was made to eliminate the oxygen since that appeared to be the greatest impurity. The shield (fig. 6) was installed to cover the interior surface of the alumina cylinder. This shield was fabricated from stainless steel even though it was recognized that this would be lossy from the rf standpoint. With this shield the rf power into the plasma was somewhat reduced, but the oxygen and aluminum were eliminated. There resulted, however, an increased intensity of the chromium and iron lines in the shield area so that one type of contamination was substituted for another.

The plasma exhibits many fluctuations that can be observed in the Langmuir-probe, magnetic-probe, diamagnetic-coil, neutural-particle-analyzer, and microwave-interferometer measurements. One of the low-frequency fluctuations (near 4 kHz) observed by Langmuir probes spaced around the periphery of the plasma indicated a plasma rotation. This rotation appeared to be a result of the $E \times B$ drift, E being the field set up by the plasma potential and B being the axial magnetic field.

Low-frequency fluctuations observed in the diamagnetic coils depended on the position of the coil. The intensity was greatest at the bottom of the beach and increased with rf power. These fluctuations were in phase throughout the apparatus.

Signals picked up by all the instrumentation exhibited a wide spectrum of frequencies. Frequencies from 1 hertz to many megahertz were noted, there being both harmonics and subharmonics.

The floating potential measured in the plasma depended on power, position, and whether or not there was a beach. With beach, the potential was always positive and was 10 to 20 volts regardless of power and position. Without beach, the potential was 50 volts negative at high power (80 kW) in the center and was about 10 volts positive at the outer edge of the plasma. At low power (45 kW) the potential was approximately 20 volts positive at the center and decreased slightly toward the wall.

WAVE PROPAGATION AND DAMPING

The existence of the ion-cyclotron wave was confirmed by magnetic-probe measurements made throughout the plasma volume. According to theory (ref. 1), three components of the wave ($\dot{B}_z$, $\dot{B}_\theta$, and $\dot{B}_r$) vary in certain ways. For axially symmetric modes, $\dot{B}_z$ should be a maximum at the center of the plasma, and its phase with respect to some fixed point should be constant across the plasma; $\dot{B}_r$ and B_θ should be maximum away from the radial center, should have zero amplitude at the center, and there should be a phase change of 180° on passing through the center. Axial variations,

however, are the same for all components; that is, any component can be used to determine an axial wavelength.

Figure 16 shows how the amplitude and phase of the $\dot{B}_z$ component varied as the probe was moved axially along the centerline of the plasma away from the outermost section of the rf coil. The near field of the rf coil was quite strong and probe measurements had to be started at about 40 centimeters from the centerplane if this field were to be avoided. Hence, all measurements reported herein are taken beyond 40 centimeters where the phase is changing linearly with distance and where the rf amplitude is relatively constant.

A typical amplitude and phase measurement is shown in figure 17. This is an actual trace from the X-Y plotter. For the particular operating condition, the wavelength was determined to be 52 centimeters and was greater than the coil wavelength (41 cm). The wave amplitude was decreasing rapidly with distance.

Figure 18 shows a typical set of amplitude data taken with four values of Ω. For clarity, the curves have been separated vertically by 25 millivolts, with the ordinate applying directly to the $\Omega = 0.968$ curve. No beach was present and the probe was located at the periphery of the plasma. This figure indicates three facts. First, there was a periodic variation in the amplitude with the peaks and valleys always occurring at the same axial position regardless of the value of Ω, except at large distances where the signal amplitude was small. These variations correlated (fig. 19) with the confining magnetic field variations (±1 percent) resulting from the spacing between the dc coils. When the dc field was at a peak, the $\dot{B}_z$ amplitude was at a valley, and vice versa. These variations were also found with the probe traversing axially on the centerline of the plasma. The variations tended to disappear at higher rf power. Second, the wave was more strongly damped for Ω nearer unity in accord with theory for either collisional or collisionless damping. Third, some strong damping mechanism such as collisional damping was occurring which removed the energy from the wave before it propagated very far. Little energy (proportional to the square of the signal amplitude) was in the wave by the time the wave reached the far beach position (approximately 120 cm).

The variation of phase with probe position for various Ω values is shown in figure 20. Note that the curves have been separated horizontally 10 centimeters for clarity, with the abscissa applying directly to the $\Omega = 0.973$ curve. The slopes of the curves are a measure of the plasma wavelengths.

Figure 21 shows how the plasma wavelengths vary with Ω for both H_2 and D_2 gas. In accordance with theory the value of Ω at which the coil wavelength and the plasma wavelength are equal is smaller for H_2 than it is for D_2.

Measurements of the radial distribution of the three wave-field components $\dot{B}_z$, $\dot{B}_r$, and $\dot{B}_\theta$ are shown in figures 22 to 24. Both amplitude and phase are shown as functions of radial position.

Figure 22 shows a $\dot{B}_z$ measurement with the arc traverse. The $\dot{B}_z$ signal amplitude peaked at the center of the plasma as expected. There was a definite variation in phase across the plasma, however. This would be expected if modes of $m > 0$ were present.

A radial traverse of the $\dot{B}_\theta$ probe is shown in figure 23. The B_θ field is peaked off center and is a minimum at the center exactly as expected. Again, the phase does vary between the edge of the plasma and the center of the plasma. Although there is a big change in phase as the probe passes through the center, the phase change was not 180^o.

The $\dot{B}_r$ signal should vary in a manner similar to the B_θ signal. Instead, the $\dot{B}_r$ signal (fig. 24) varies almost like the $\dot{B}_z$ signal. The conclusion is that several wave modes are present. The rf coil cannot be constructed to give the exact current distribution used in theoretical consideration. Hence, some other mode, such as the $m = 1$ mode (ref. 23), may be present. What effect these noticeable variations in the wave fields have on the wave damping process is unknown.

Measurements were made with the total $\dot{B}_z$ probe which sums the $\dot{B}_z$ field across the plasma. A set of measurements is shown in figure 25 where both phase and amplitude are plotted for two different values of Ω, one of which is a condition to give the 41-centimeter coil wavelength. The figures show two facts: (1) there were no fluctuations in signal amplitude due to the axial variation in dc magnetic field as was observed with the local magnetic field probes, and (2) as the probe passes the nodal point the primary wave was no longer the dominant wave. Other disturbances or minor secondary waves affect the phase measurement.

Note that in figure 25(b) the amplitude is essentially zero at the node. Local magnetic probe $\dot{B}_z$ signals would have considerable amplitude at the same axial position. Apparently there was destructive interference of all the modes present in the plasma at that point.

The local magnetic field probe and the total $\dot{B}_z$ probe measurements indicate the complex nature of the wave phenomena.

As the ion cyclotron waves propagate into the decreasing magnetic field of the beach and approach the $\Omega = 1$ point, ion cyclotron damping increases. Wave energy is converted into ion kinetic energy. The probe measurements reveal the general features of wave damping in the beach.

Figure 26 shows the affect of the beach on probe signal amplitude. As the wave moved into the decreasing magnetic field, energy was transferred to the ions and the signal amplitude decreased. The wave energy (proportional to square of signal amplitude) was essentially zero at the bottom of the beach.

As the wave moved into the beach, the phase angle also changed (fig. 27) and the wavelength as determined from the slope of the curve was continuously shortening. Near

the $\Omega = 1$ point the phase angle changed linearly with distance indicating a wavelength of 12.5 cnetimeters. Although the signal amplitude was small at this point and in fact might not be a good measurement of the wave, the wavelength was in agreement with the minimum wavelength calculations using equations in reference 9.

ION HEATING AND CONTAINMENT

As the ion cyclotron waves propagated into the decreasing magnetic field of the beach, they reached a point where $\Omega = 1$. The waves should be damped before this point is reached and the energy of the wave should be directly converted into ion kinetic energy. The ion motion should be initially perpendicular to the magnetic field. Because of this perpendicular motion, the ions are trapped in the small local magnetic mirror.

Any of the measurements of ion temperature quoted as a maximum temperature are taken at the magnetic field that gives the greatest perpendicular pressure. Generally, this field is not that at which maximum rf power transfer is observed. Figure 28 shows that the maximum of the perpendicular pressure curve occurred at somewhat greater magnetic fields than did the maximum of the rf power curve. This may be the result of more power being propagated to the beach under this condition. These data were taken at low power and consequently low density so that the operating Ω was such that the wave encountered the $\Omega = 1$ point before the bottom of the beach was reached.

Experimental measurements of the ion temperature in the magnetic beach are shown in figure 29. For this particular operating condition, the ion temperature was 500 electron volts and the ion density was 2×10^{12} cubic centimeters. The peak temperature always occurs at the minimum field position in the beach.

Measurements were made of the electron density decay times and of the ion energy decay time. Figure 30 shows the time history of the electron density (microwave) after rf transmitter was unkeyed. The density remained constant for about 400 microseconds after unkeying and then reached 1/e of the steady-state density about 400 microseconds later. During this period the electrons have sufficient energy to maintain ionization. As shown in figure 31, the ion energy decay time was about 100 microseconds. This decay time did not vary markedly over the range of conditions of this apparatus. Energy decay due to charge exchange depends on the local neutral density which is not known. However, for neutral densities in the 10^{11} to 10^{12} range, energy decay times of the order of 100 microseconds would be expected. Containment time by the Bohm equation is calculated to be slightly greater than 200 microseconds.

Table I shows a comparison of results obtained with H_2 (6.5 and 10 MHz) and D_2 (6.5 MHz). Operating at a higher frequency or a higher field gives greater efficiency

and greater perpendicular pressure. It should be noted that at greater power (70 kW) the efficiency with D_2 does increase to 73 percent. Higher power with H_2 at 10 MHz was not used because coil voltages become too great at higher frequencies. This increase results from lower coil Q at the higher frequencies.

One difficulty in using the diamagnetic signals for ion temperature measurement is that the plasma density also has to be determined. Langmuir probes that were used for this determination could not be relied on to give the density to within a factor of 2. Because the diamagnetic measurement and the neutral particle measurement were more reliable, it was decided to calculate the plasma density from these two measurements. At 90 kilowatts the energy density was determined to be 3.96×10^{15} electron volts per cubic centimeter (after corrections for resolution of the diamagnetic coil) and the neutral particle measurement resulted in a temperature of 870 electron volts. The density calculates to be 4.6×10^{12} ions per cubic centimeter.

Neutrons were observed coming from the beach regions when the power level was above 45 kilowatts. An attempt was made to see how well the production rate agreed with the ion temperature measurements. Figure 32 shows a calculation of the neutron flux expected at the detector position as a function of density and temperature. At 90 kilowatts, a neutron flux of 15 neutrons per square centimeter per second was measured. With a density of 4.6×10^{12} ions per cubic centimeter, this flux corresponds to an ion temperature of 600 electron volts. This is lower than the neutral particle measurement indicates. Little reliance is placed on the nuclear measurement until further information on the temperature distribution and on the nuclear production process is available.

There is evidence for considerable energy losses throughout the whole system. Wave measurements showed that wave damping was occurring even when the beach was not present. Spectrographic measurements indicated strong bombardment of the alumina section and of the walls of the beaches. Some data have been obtained that show these losses.

Figure 33 shows the results of power balance measurements made on the oil-cooled center section. The plasma power that is absorbed by the center section depends on Ω and is greater as Ω becomes nearer unity. This is an expected trend, since wave damping increases as Ω approaches unity and more energy is removed nearer the rf coil. The figure does show the importance of operating at small Ω as energy absorbed in the center section is not available for the wave propagation to the beaches.

For a certain test in which 20 kilowatts was transferred to the plasma, 10 kilowatts went into the alumina tube and 5 kilowatts went into each of the two arms. Figure 34 shows the distribution of energy flux to a water-cooled wall of the arm of the apparatus. As water flowed toward the center of the system (from right to left in fig. 34) it absorbed energy lost from the plasma. The ordinate is the power absorbed by the water

as it flows from the entrance to the point of interest. The accumulated heat transfer is determined from the temperature rise and the mass flow rate of the water. The slope of the curve is proportional to the heat flux at that point.

There is little difference between the curves obtained for no-beach and far-beach operation (upper curve of fig. 34). Since the wave was damped before reaching the beach position, it is logical that inserting a beach would have negligible effect. The data show that 3 kilowatts was lost between the rf section and the grid and 2 kilowatts in the vicinity of, or just beyond, the grid. Apparently, as the wave energy was damped, hot neutrals carried the energy to the walls.

If the near beach is used, an effect on heat transfer should be observed, since the wave is strong and damping it should change the temperature distribution. Such a change is found in the lower curve of figure 34; the energy is shown going to the wall at a much greater rate between the rf section and the grid. Energy goes to the wall in this region probably by means of the charge-exchange neutrals.

CONCLUDING REMARKS

A number of conclusions have been reached as a result of this program:

1. Consistent with theoretical predictions, rf power can be coupled with good efficiency (~70 percent) to the plasma. The resulting ion temperature was about 870 electron volts and the density was about 5×10^{12} ions per cubic centimeter with a total rf power of 90 kilowatts. In this range of temperature and density, the apparatus used in these studies provides a steady and reproducible source of plasma.

2. Grid structures are extremely important to the coupling process. They appear to act as a source of atomic hydrogen.

3. The critical problem for running high rf power (~120 kW) is the heating of an aluminum oxide center section tube. A cooled shield could eliminate this problem. Increased breakdown resistance is also needed either by increasing the breakdown strength of the insulating gas in an rf section or by using a thicker outer aluminum oxide tube.

4. Wave measurements, while generally consistent with theoretical predictions, show details difficult to reconcile with any single axisymmetric wave in the plasma.

5. No major differences are found between data taken with this rf-sustained mode and with the pulse systems.

6. Reproducibility of plasma conditions was quite good even though at the maximum power there were very strong plasma fluctuations that made measurements difficult.

7. Plasma contamination from either the center section or the beach region does not appear to play a strong role in power absorption or wave propagation.

Lewis Research Center,
National Aeronautics and Space Administration,
Cleveland, Ohio, December 6, 1972
503-10.

REFERENCES

1. Stix, Thomas H.: Oscillations of a Cylindrical Plasma. Phys. Rev., vol. 106, no. 6, June 15, 1957, pp. 1146-1150.

2. Stix, T. H.; and Palladino, R. W.: Ion Cyclotron Resonance. Theoretical and Experimental Aspects of Controlled Nuclear Fusion. Vol. 31 of the Proceedings of the Second United Nations International Conference on the Peaceful Uses of Atomic Energy. United Nations, 1958, pp. 282-287.

3. Hooke, William M.; and Rothman, Milton A.: A Survey of Experiments on Ion Cyclotron Resonance in Plasma. Nucl. Fusion, vol. 4, no. 1, Mar. 1964, pp. 33-47.

4. Swett, Clyde C.; and Krawec, Roman: Experiments on Ion-Cyclotron Wave Generation, Using an Electrostatically Shielded RF Coil. Bull. Am. Phys. Soc., vol. 10, no. 4, Apr. 1965, p. 509.

5. Swett, Clyde C.: Effect of Magnetic Beach on RF Power Absorption in Ion Cyclotron Resonance. Bull. Am. Phys. Soc., vol. 11, no. 4, June 1966, p. 450.

6. Swett, Cylde C.; and Krawec, Roman: Operation of an Ion-Cyclotron-Wave-Generation Apparatus in an RF Self-Sustained Mode. Bull. Am. Phys. Soc., vol. 13, no. 2, Feb. 1968, p. 278.

7. Sigman, Donald R.; Krawec, Roman; Hettel, Henry J.; and Swett, Clyde C.: Further Experiments on Ion-Cyclotron Wave Generation in the RF Self-Sustained Mode. Bull. Am. Phys. Soc., vol. 13, no. 11, Nov. 1968, p. 1509.

8. Swett, Clyde C.: Thermalization of Ion-Cyclotron Waves in a Magnetic Beach. Bull. Am. Phys. Soc., vol. 14, no. 11, Nov. 1969, p. 1020.

9. Uman, Myron F.; and Hooke, William M.: Observation of Ion Cyclotron Waves in a Hot Plasma. Phys. Fluids, vol. 12, no. 5, May 1969, pp. 1072-1080.

10. Kristiansen, Magne; and Dougal, Arwin A.: Experimental Investigation of Harmonic Ion Cyclotron Wave Propagation and Attenuation. Phys. Fluids, vol. 10, no. 3, Mar. 1967, pp. 596-604.

11. Swett, Clyde C.: Experiments on Inductive and Capacitive Radiofrequency Heating of a Hydrogen Plasma in a Magnetic Field. NASA TN D-2717, 1965.

12. Swett, Clyde C.; and Krawec, Roman: Preliminary Observations of RF Power Transfer to a Hydrogen Plasma at Frequencies Near the Ion Cyclotron Frequency. Engineering Aspects of MHD. N. W. Mather and G. W. Sutton, eds., Gordon and Breach Sci. Publ., 1964, pp. 599-614.

13. Hettel, Henry J.; Krawec, Roman; Prok, George M.; and Swett, Clyde C.: Enhancement of Ion Cyclotron Waves in Hydrogen Helium Mixtures. NASA TN D-4271, 1968.

14. Sigman, Donald R.; and Reinmann, John J.: Ion Cyclotron Wave Generation in Uniform and Nonuniform Plasma Including Electron Inertia Effects. NASA TN D-4058, 1967.

15. Sigman, Donald R.: Some Limitations on Ion-Cyclotron Wave Generation and Subsequent Ion Heating in Magnetic Beaches. NASA TM X-2263, 1971.

16. Sigman, Donald R.: Radiofrequency Power Transfer to Ion-Cyclotron Waves in a Collision-Free Magnetoplasma. NASA TN D-3361, 1966.

17. Reinmann, John J.; and Sigman, Donald R.: Cyclotron Waves in a Two-Ion Species Plasma. Bull. Am. Phys. Soc., vol. 13, no. 2, Feb. 1968, p. 270.

18. Hooke, W. A.; Rothman, M. A.; Sinnis, J.; and Adam, J.: Temperature and Power Measurements in a Plasma Heated by Absorption of Ion Cyclotron Waves. Phys. Fluids, vol. 8, no. 6, June 1965, pp. 1146-1154.

19. Vasil'ev, M. P.; Grigor'eva, L. I.; Dologopolov, V. V.; Smerdov, B. I.; Stepanov, K. N.; and Chechkin, V. V.: Experimental Study of the Absorption of High-Frequency Energy by a Plasma at Ionic Cyclotron Resonance. II. Soviet Phys.-Tech. Phys., vol. 9, no. 6, Dec. 1964, pp. 762-768.

20. Shvets, O. M.; Tarasenko, V. F.; Ovchinnikov, S. S.; Brzhechko, L. V.; Pavlichenko, O. S.; and Tolok, V. T.: High-Frequency Heating of a Dense Plasma in a Metal Chamber. Soviet Phys.-Tech. Phys., vol. 11, no. 3, Sept. 1966, pp. 328-330.

21. Nazarov, N. I.; Ermakov, A. I.; and Tolok, V. T.: High-Frequency Heating of a Dense Plasma. Soviet Phys.-Tech. Phys., vol. 11, no. 4, Oct. 1966, pp. 459-464.

22. Woollett, Richard R.: Energy Addition to an Atomic Hydrogen Plasma at Off-Resonant Conditions. NASA TN D-2982, 1965.

23. Sigman, Donald R.: A Comparison of Coupling Efficiencies for a Stix Coil and an M = 1 Coil. NASA TM X-2547, 1972.

24. Phillips, R. C.; and Turner, E. B.: Construction and Calibration Techniques of High Frequency Magnetic Probes. Rev. Sci. Instr., vol. 36, no. 12, Dec. 1965, pp. 1822-1825.

25. Rothman, M. A.: Measurement of Plasma Diamagnetism by a Coil Located Near a Conducting Wall. Plasma Phys., vol. 10, no. 1, Jan. 1968, pp. 86-91.

26. Krawec, Roman: Evaluation of Ion Density and Plasma Potential from Langmuir Probe Data. NASA TM X-2369, 1971.

27. Drawin, H. W.: Mass Spectrometry of Plasmas. Plasma Diagnostics. W. Lochte-Holtgreven, ed., North-Holland Publ. Co., 1968, p. 801.

28. Langmuir, Irving: A Chemically Active Modification of Hydrogen. Low Pressure Phenomena. Vol. 1 of the The Collected Works of Irving Langmuir. Pergamon Press, 1960, pp. 68-82.

29. von Engel, A.: Ionized Gases. Oxford Univ. Press, 1955, p. 55.

TABLE I. - COMPARISON OF OPERATING CONDITIONS

	Hydrogen (H_2) at		Deuterium (D_2) at 6.5 MHz
	6.5 MHz	10 MHz	
Magnetic field, T	0.476	0.747	0.920
Frequency ratio, Ω	0.895	0.878	0.926
Total power, P_T	45.0	41.0	45.0
No plasma power, P_0	16.0	10.7	15.4
Plasma power, P_p	29.0	30.3	29.6
Efficiency, P_p/P_T, percent	64.5	73.9	65.8
Perpendicular pressure, P, eV/cm^3	4.62×10^{14}	9.76×10^{14}	1.00×10^{15}

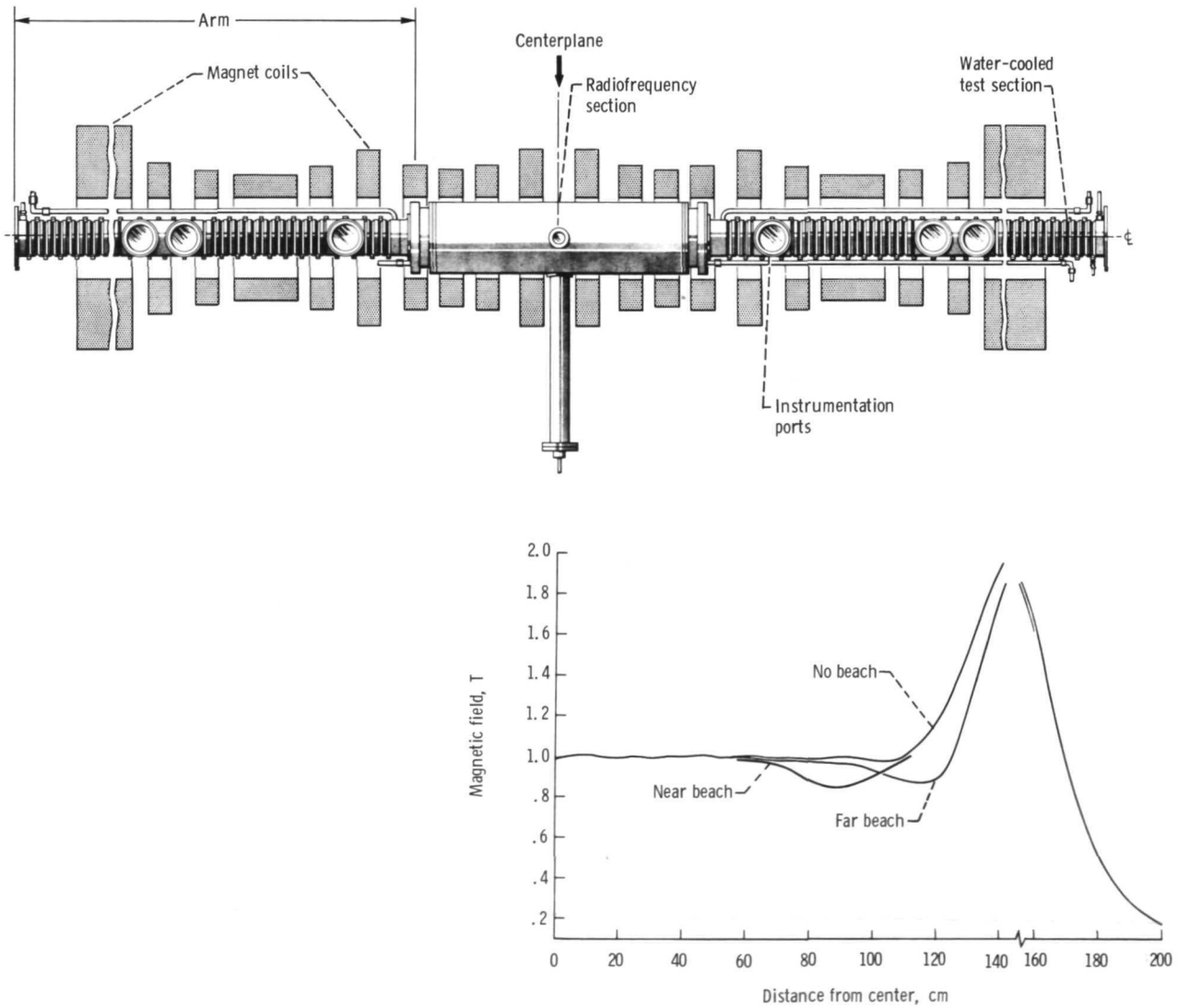

Figure 1. - Magnetic field and vacuum-chamber configuration.

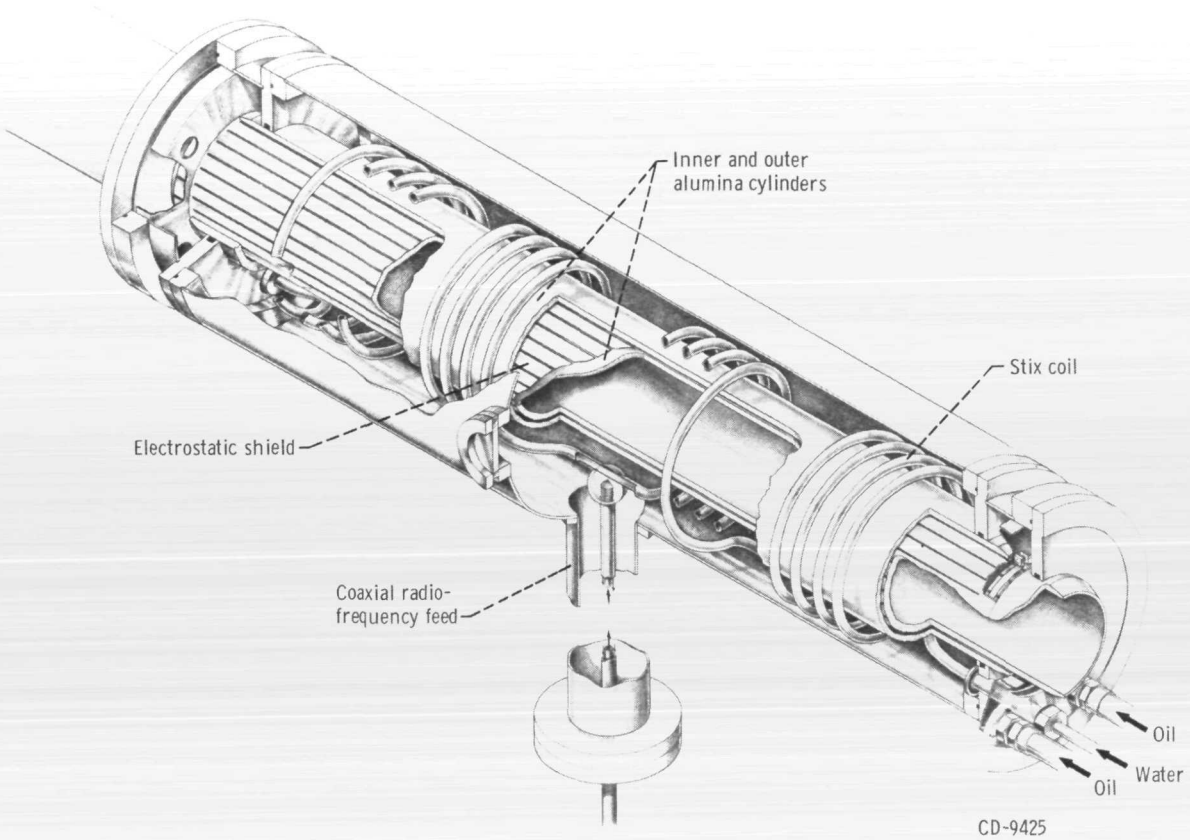

Figure 2. - Radiofrequency section.

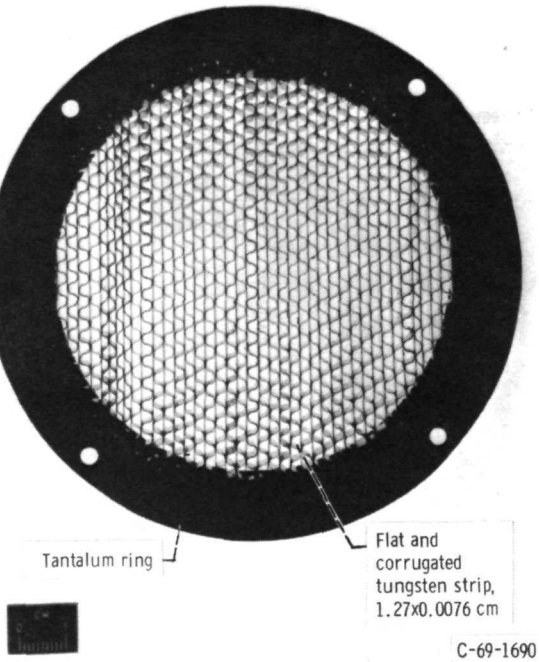

(a) Straight grid - type II arm.

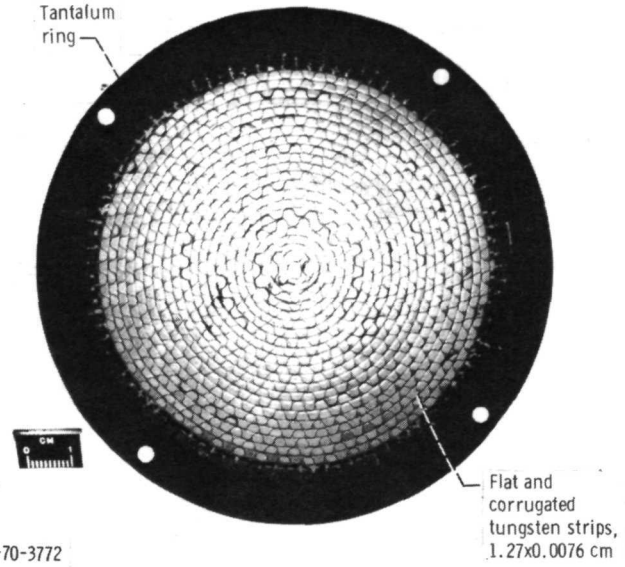

(b) Circular grid - type II arm.

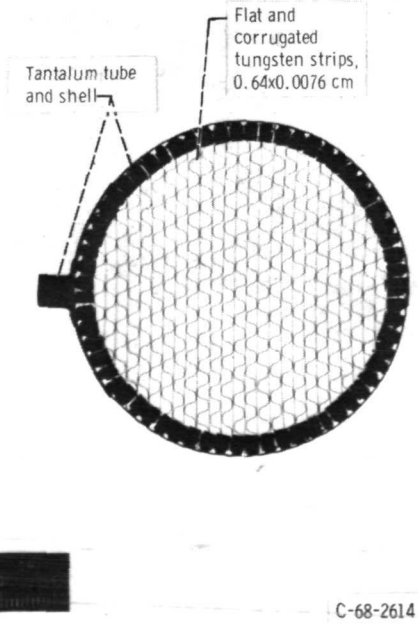

(c) Grid - type I arm.

Figure 3. - Grid structures.

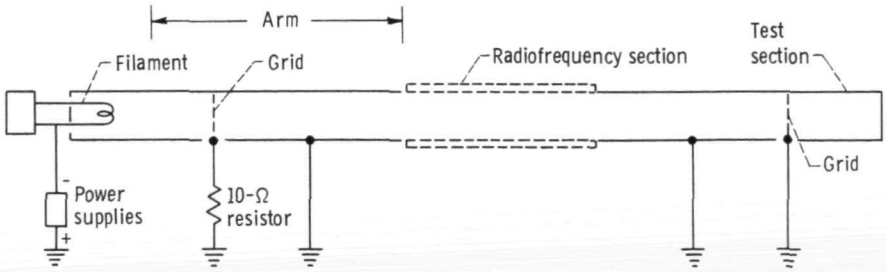

Figure 4. - Electrical connections to grids.

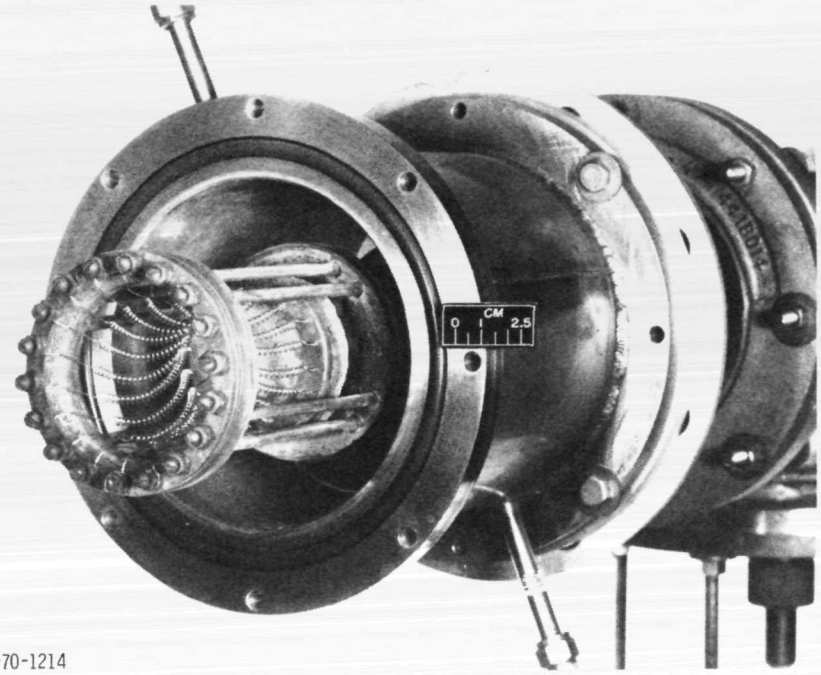

C-70-1214

Figure 5. - Filament structure.

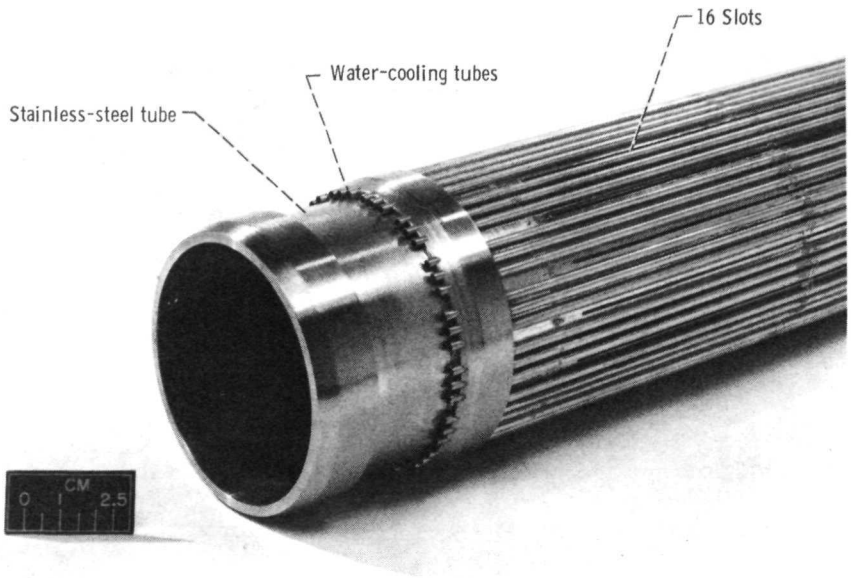

C-71-824

Figure 6. - Water-cooled shield placed inside radiofrequency section for oxygen reduction test.

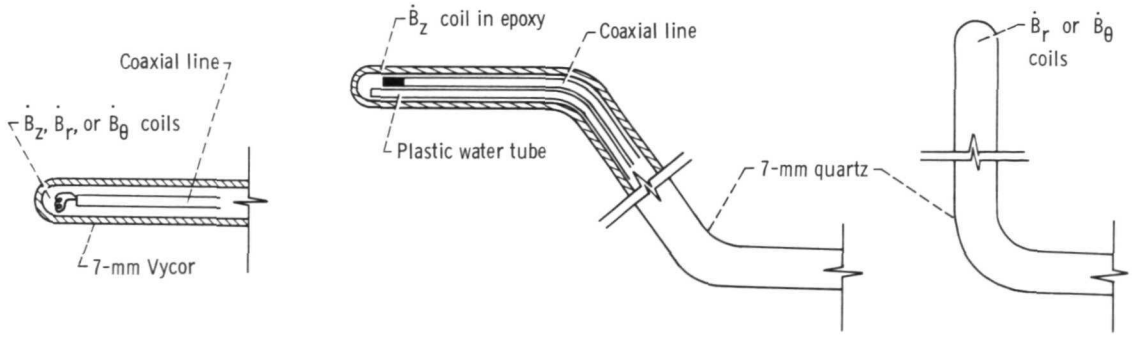

(a) Radial-traverse probe.

(b) Arc-traverse probes.

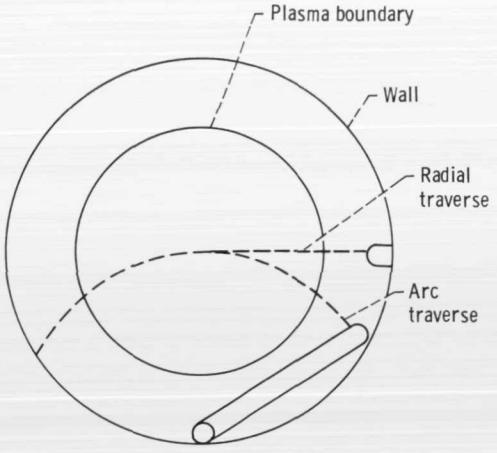

(c) Paths of probes.

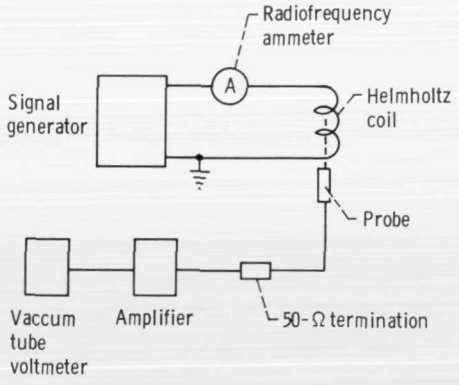

(d) Calibration circuit.

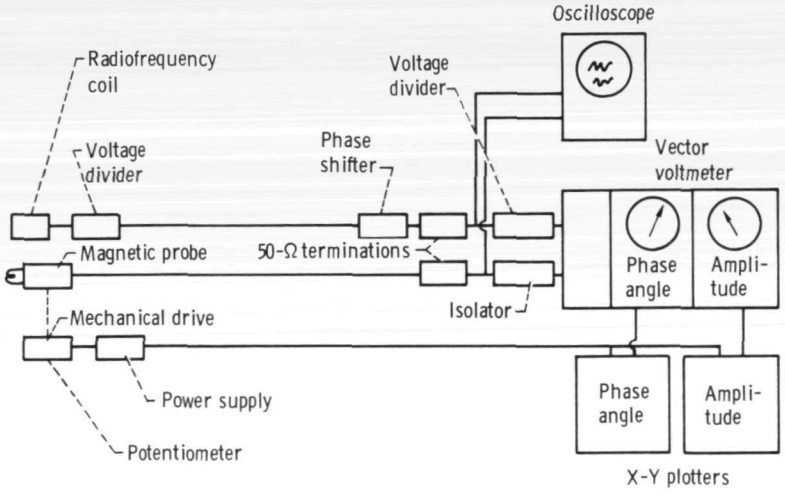

(e) Probe-readout block diagram.

Figure 7. - Magnetic-probe details.

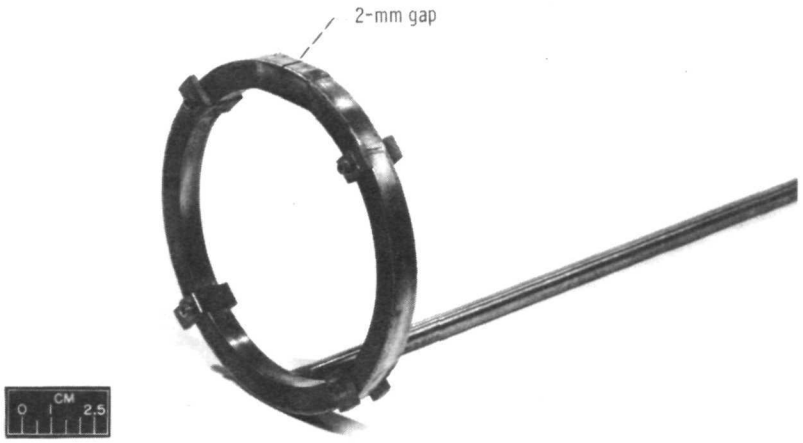

C-72-913

Figure 8. - Total $\dot{B}_2$ probe.

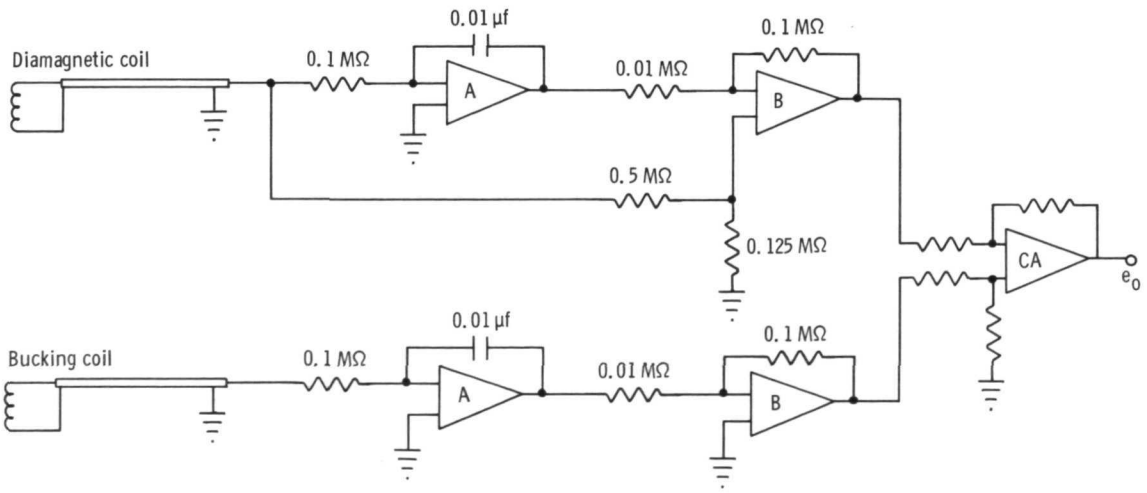

Figure 9. - Circuit for plasma-diamagnetism measurements.

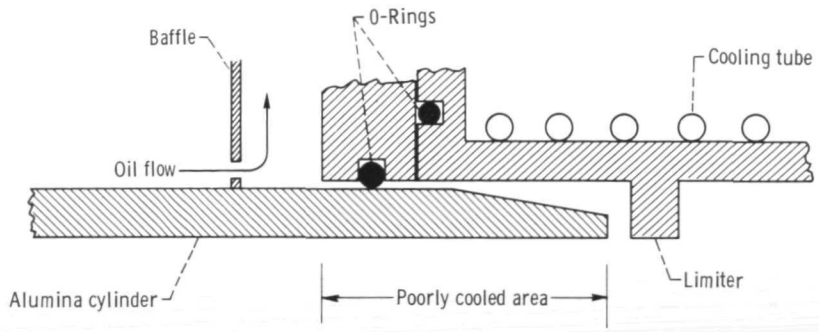

Figure 10. - Detail at end of inner alumina cylinder.

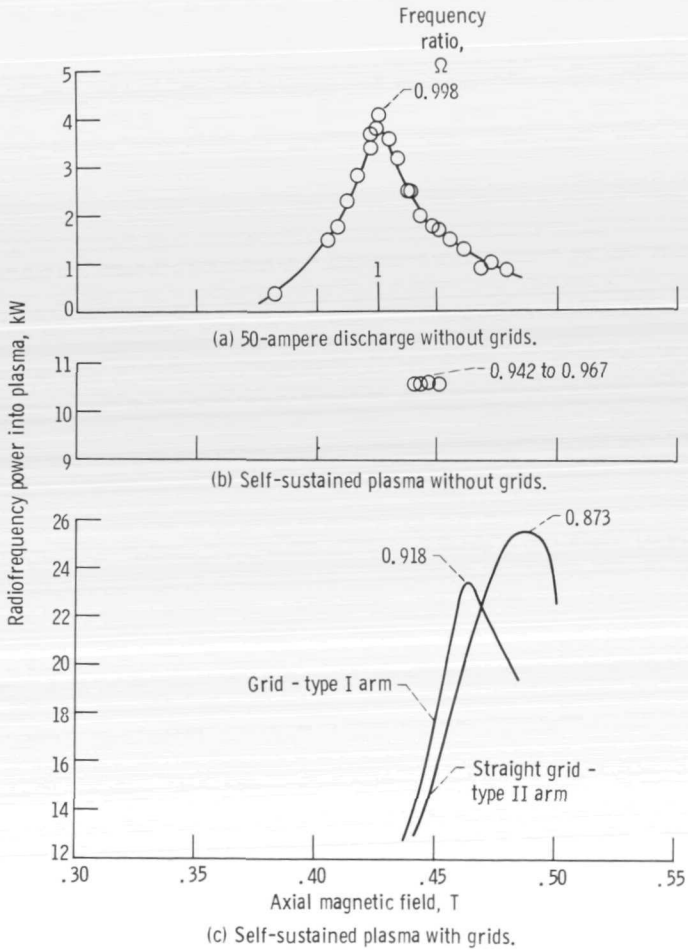

Figure 11. - Radiofrequency power absorbed by plasma for different methods of operation. Coil current, 200 amperes; no beach; gas, hydrogen (H_2).

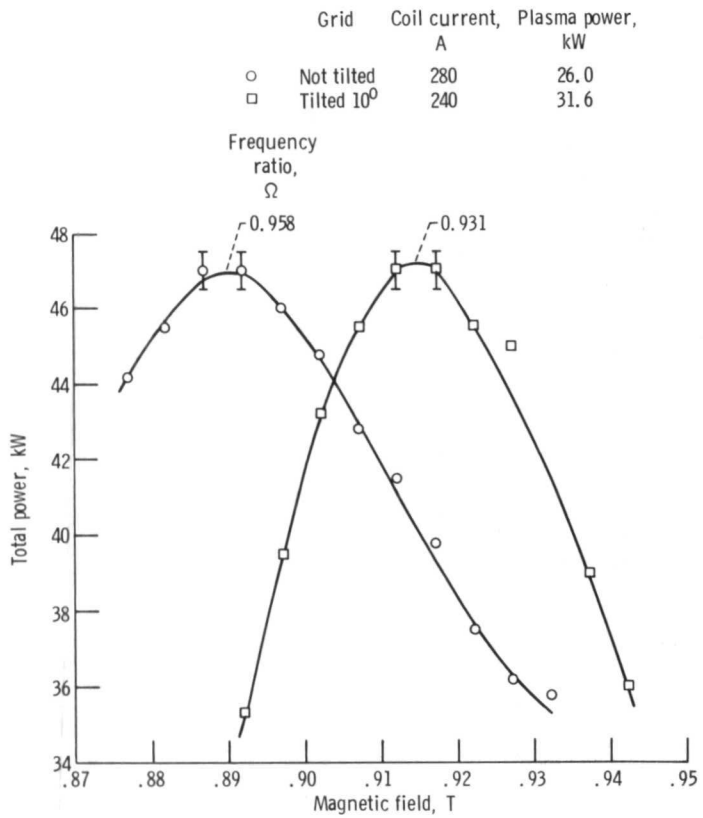

Figure 12. - Effect of grid tilting on radiofrequency power for deuterium.

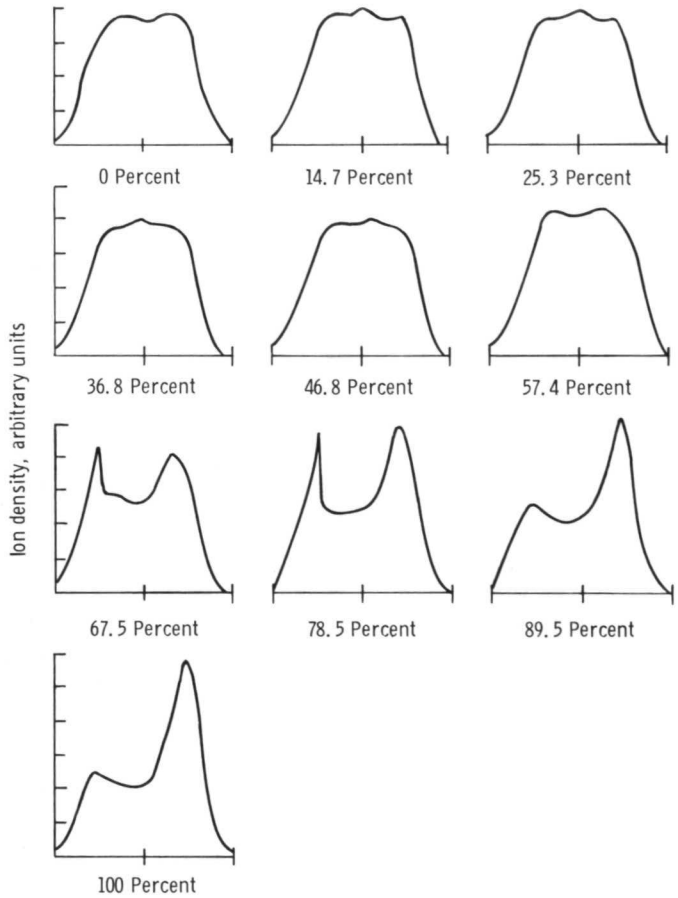

Figure 13. - Ion-density profiles at bottom of beach for various fractions of full beach. Divisions are 20 milliamperes each; 0 percent indicates no beach while 100 percent indicates full beach; 20 milliamperes $\simeq 0.85 \times 10^{12}$ per cubic centimeter assuming electron temperature T_e is 12 electron volts, radiofrequency power is 45 kilowatts, frequency ratio Ω is 0.895, and gas is hydrogen (H_2).

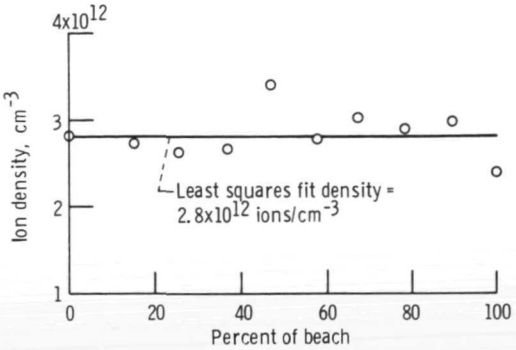

Figure 15. - Average ion density in beach. Radio-frequency power, 45 kilowatts; frequency ratio, $\Omega = 0.895$; gas, hydrogen (H_2).

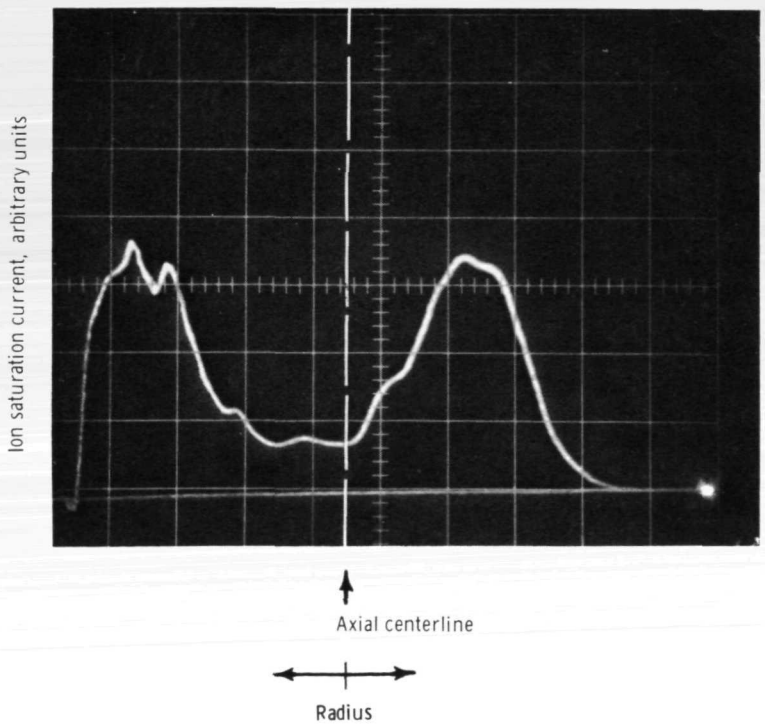

Figure 14. - Radial ion-density profile with correctly tilted grid.

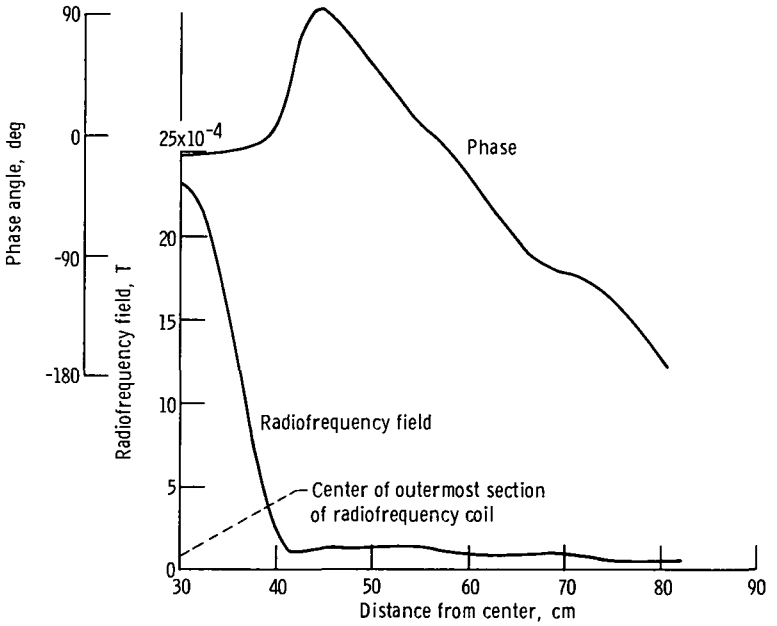

Figure 16. - Radiofrequency field and phase measurements in center of plasma. Coil current, 170 amperes; frequency ratio, $\Omega = 0.922$; no beach; $\dot{B}_z$ probe.

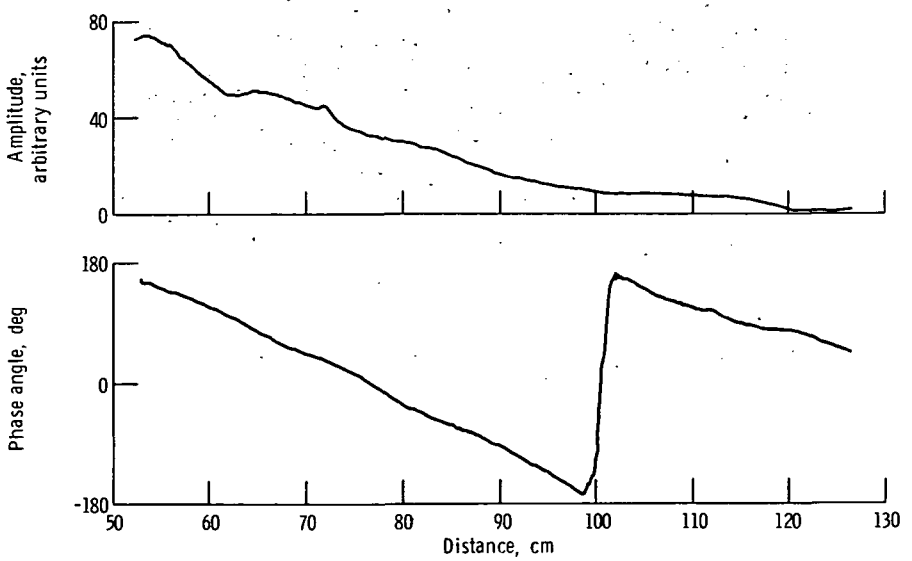

Figure 17. - Typical amplitude and phase measurement - axial traverse. Radiofrequency power, 19.8 kilowatts; frequency ratio, $\Omega = 0.945$; gas, hydrogen (H_2); no beach; $\dot{B}_z$ probe.

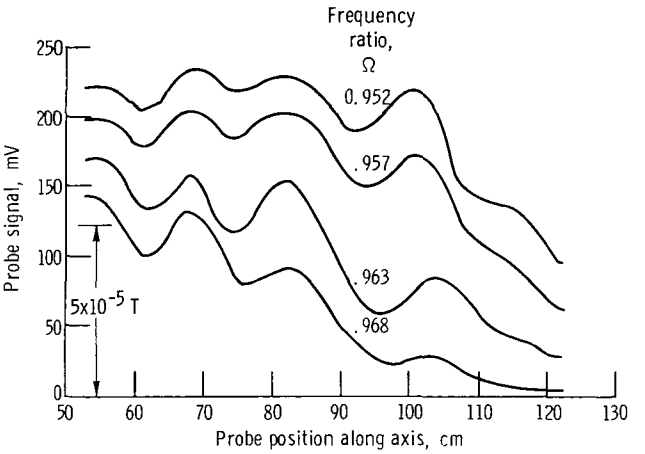

Figure 18. - Amplitude of $\dot{B}_z$ as function of axial position for four values of frequency ratio Ω. Radiofrequency current, 140 amperes; gas, hydrogen (H_2); no beach; curves separated vertically 25 millivolts.

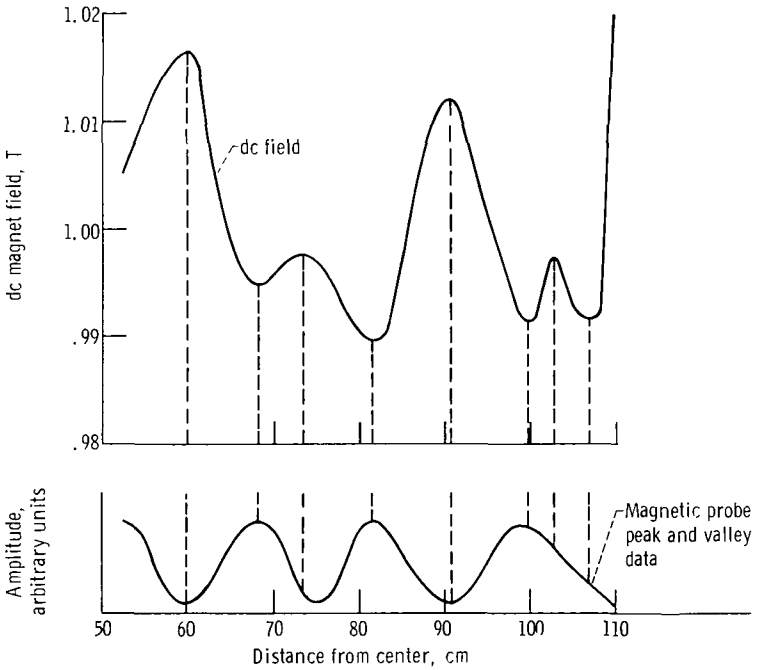

Figure 19. - Correlation of $\dot{B}_z$ magnetic probe signal amplitude with dc magnetic field.

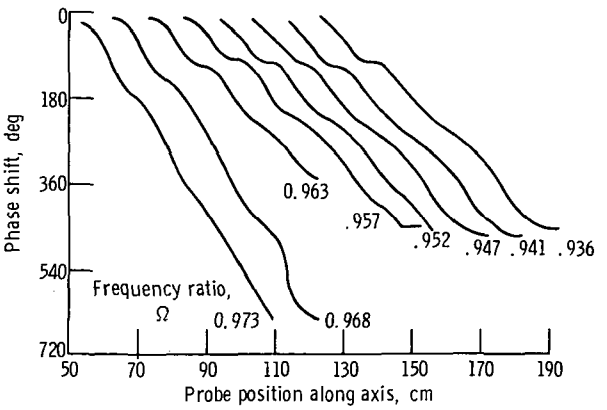

Figure 20. - Phase of $\dot{B}_z$ as function of axial position for eight values of frequency ratio Ω. Radiofrequency current, 170 amperes; gas, hydrogen (H_2); no beach; curves separated 10 centimeters horizontally.

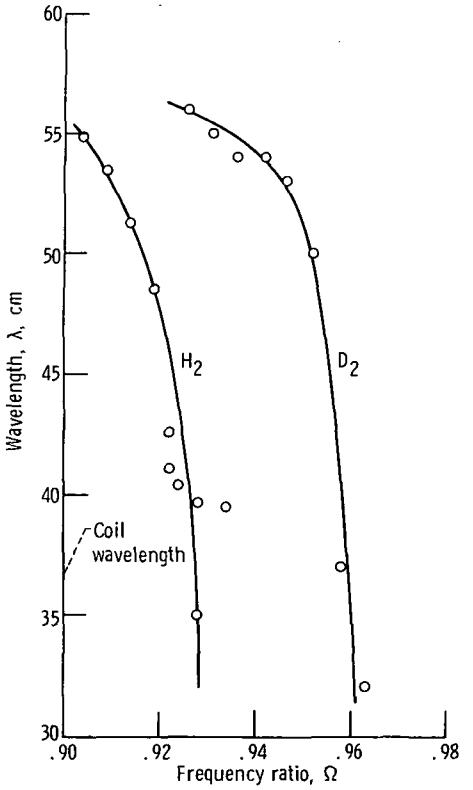

Figure 21. - Effect of Ω on wavelength λ for hydrogen (H_2) and deuterium (D_2). Density, approximately 1×10^{12} to 2×10^{12} per cubic centimeter.

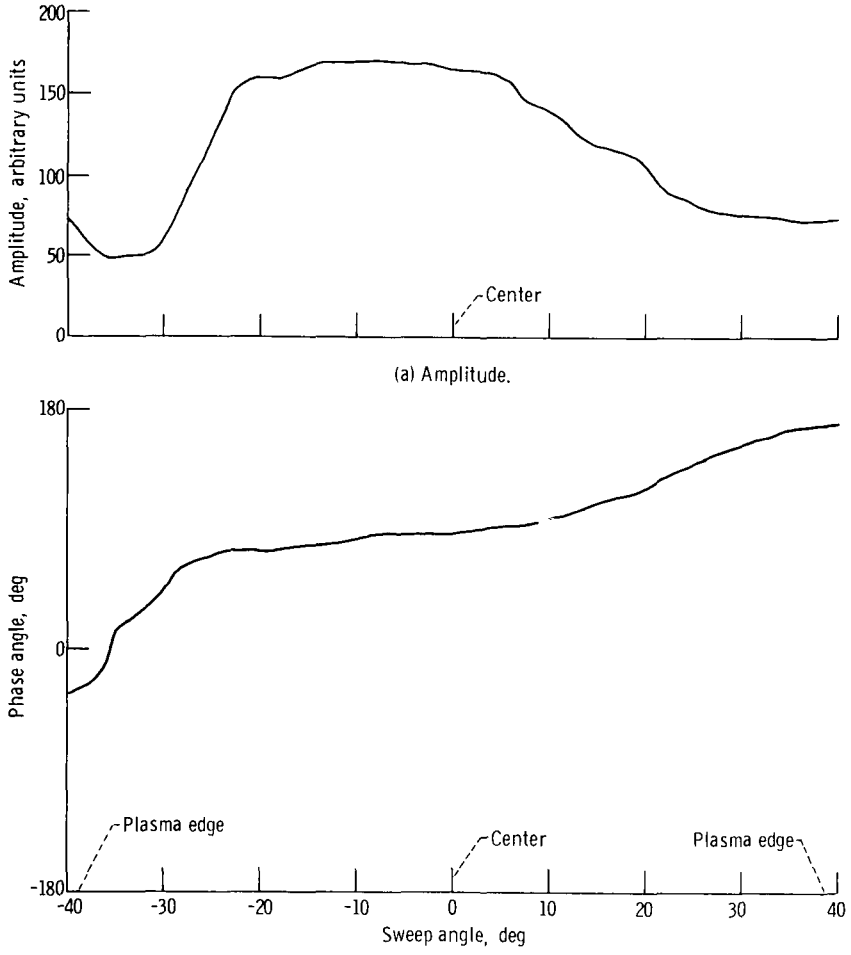

Figure 22. - Amplitude and phase measurement - arc traverse. Radiofrequency power, 43 kilowatts; frequency ratio, $\Omega = 0.927$; gas, deuterium (D_2); no beach; $\dot{B}_z$ probe; axial position, 70 centimeters from centerplane.

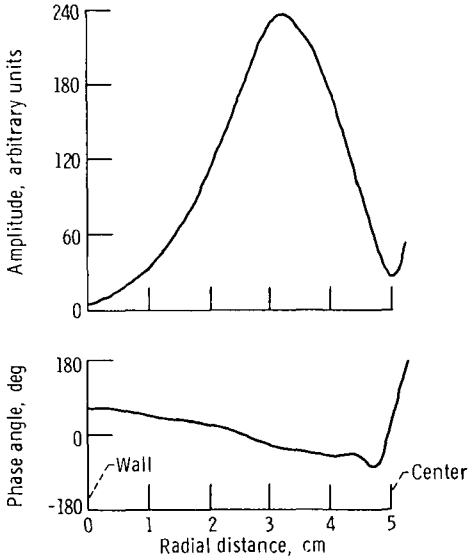

Figure 23. - Typical amplitude and phase measurement - radial traverse. Radiofrequency power, 20 kilowatts; frequency ratio, $\Omega = 0.945$; gas, hydrogen (H_2); no beach; B_θ probe; axial position, 70 centimeters from centerplane.

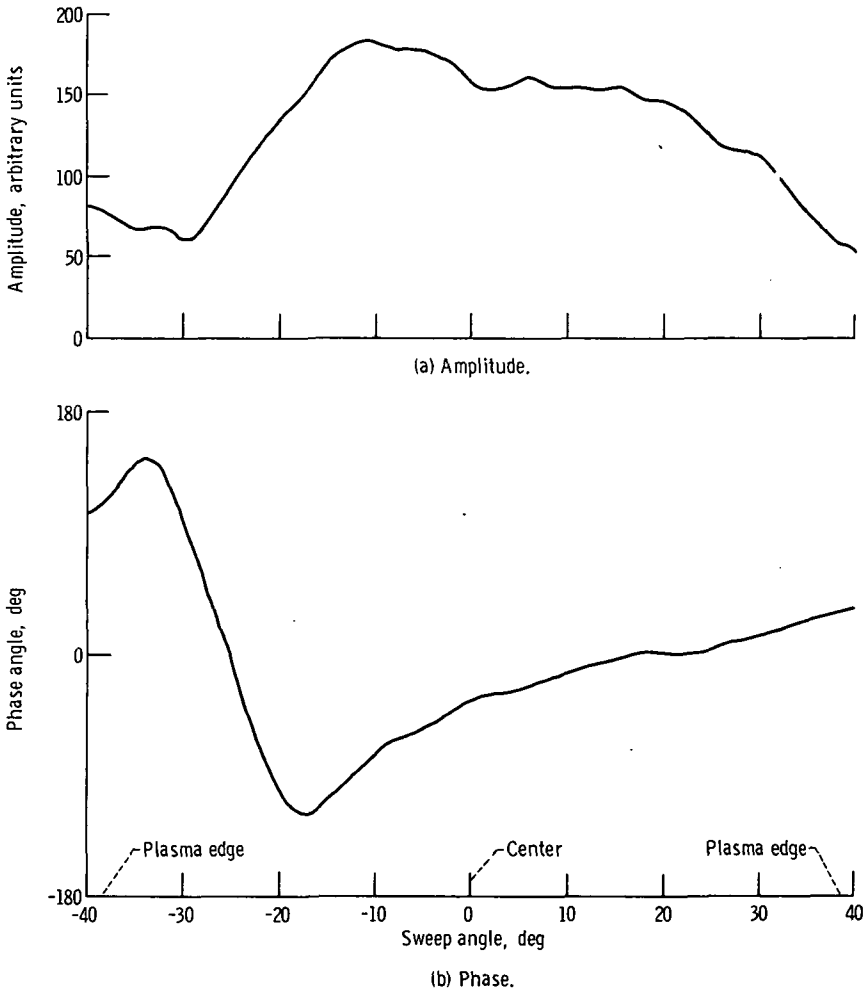

Figure 24. - Amplitude and phase measurement - arc traverse. Radiofrequency power, 42 kilowatts; frequency ratio, $\Omega = 0.927$; gas, deuterium (D_2); no beach; $\dot{B}_r$ probe; axial position, 70 centimeters from centerplane.

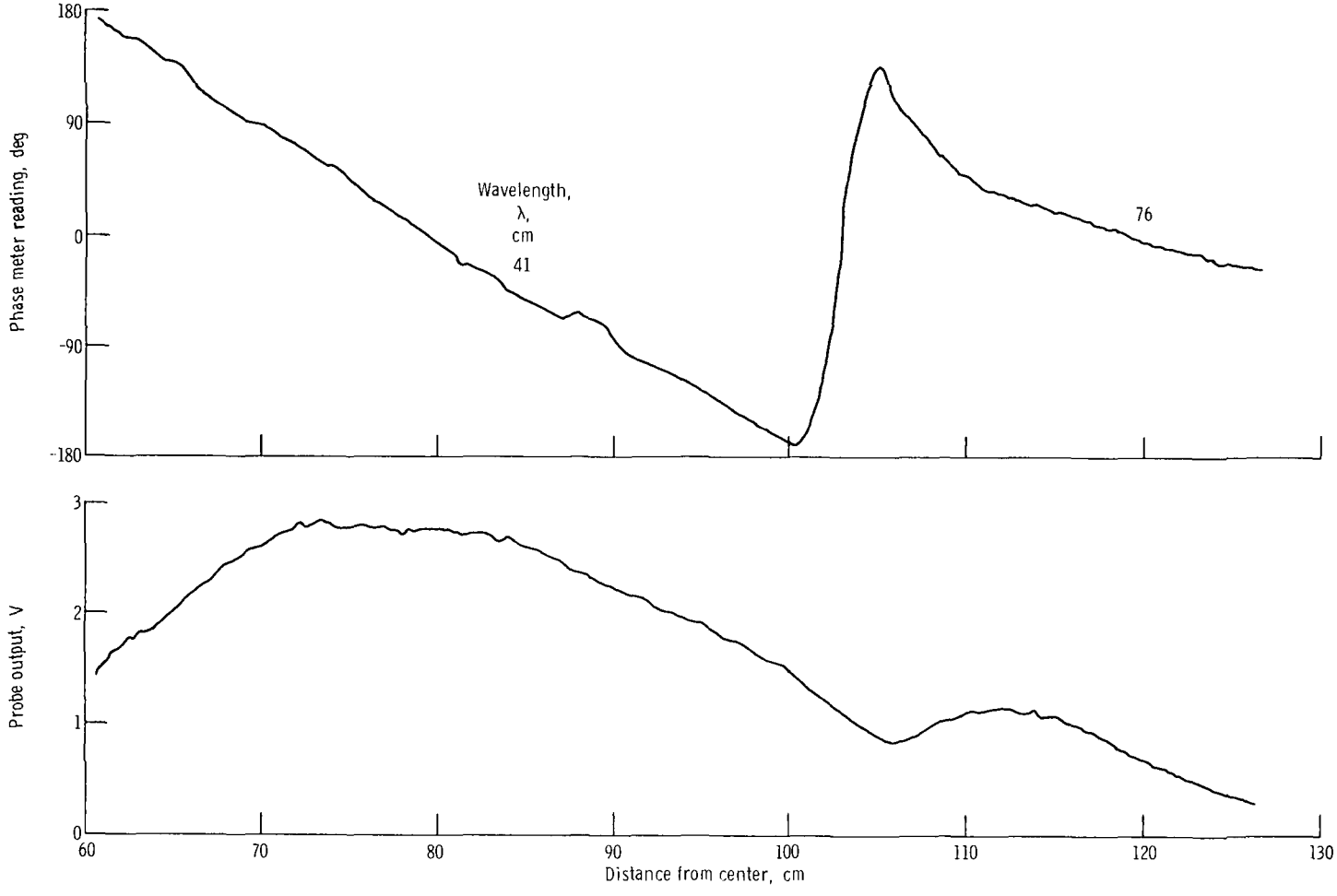

(a) Frequency ratio, $\Omega = 0.93$.

Figure 25. - Total $\dot{B}_z$ probe amplitude and phase measurements. Radiofrequency power, 45 kilowatts; gas, deuterium (D_2).

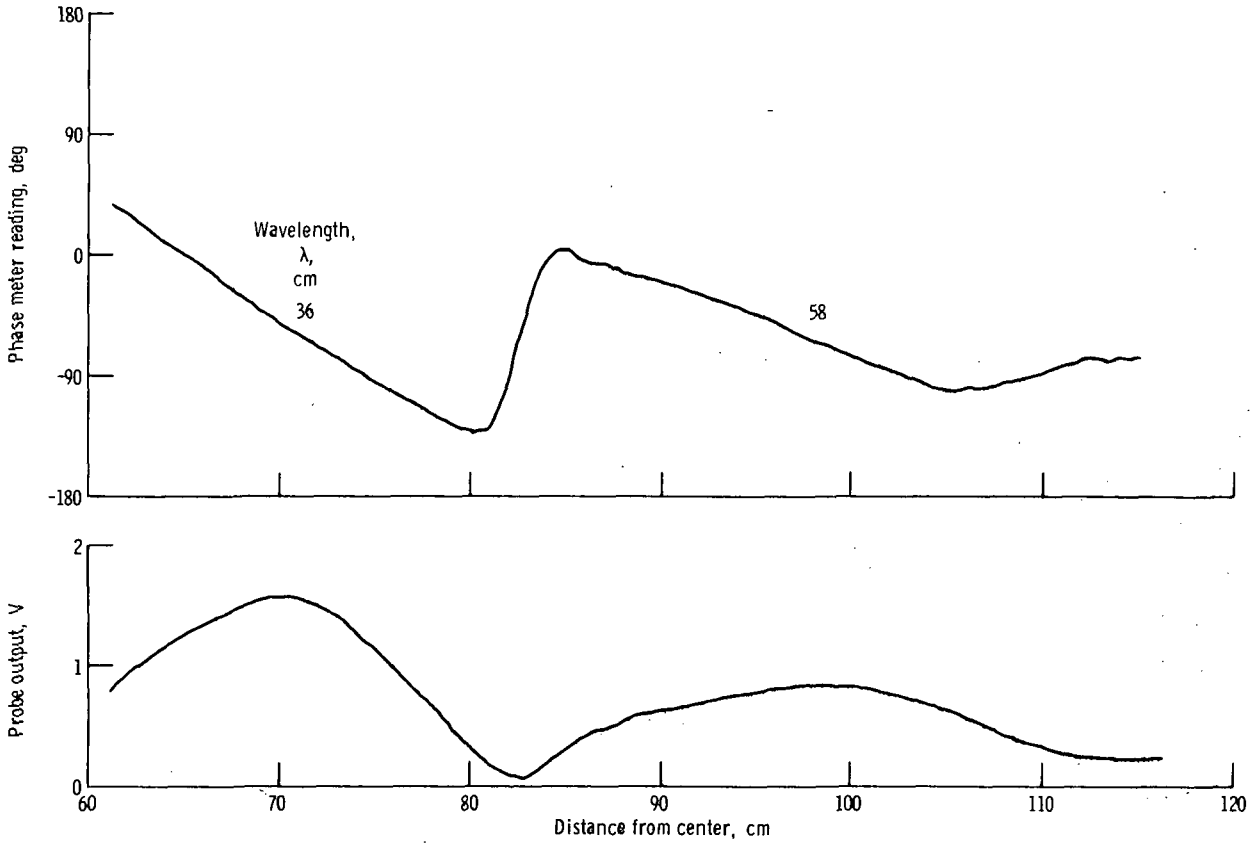

(b) Frequency ratio, $\Omega = 0.96$.

Figure 25. - Concluded.

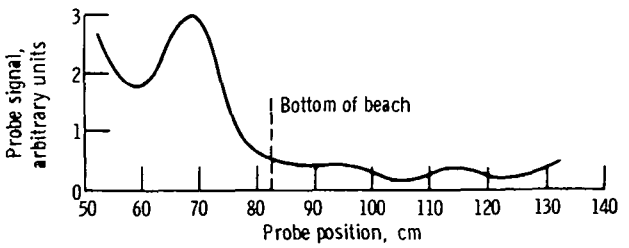

Figure 26. - Effect of near beach on $\dot{B}_z$ probe signal amplitude. Radiofrequency current, 200 amperes; frequency ratio, $\Omega = 0.934$; gas, hydrogen (H_2).

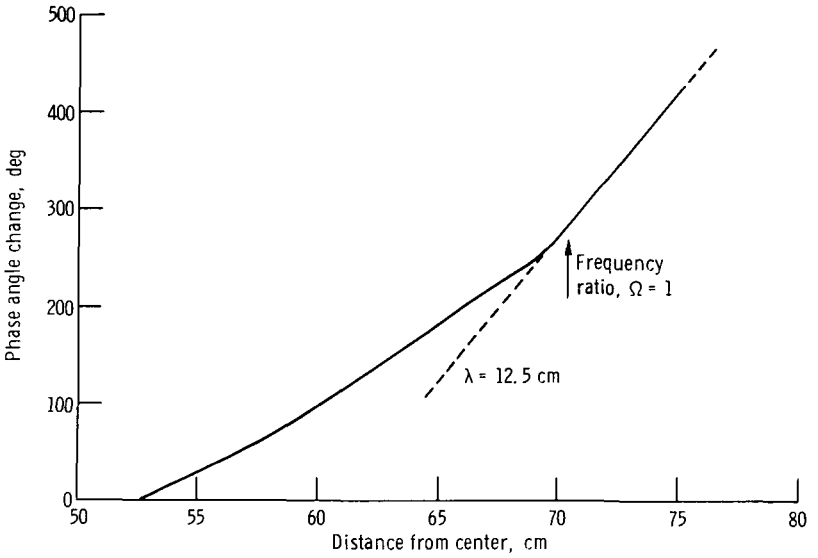

Figure 27. - Change in phase angle as wave enters beach. At radiofrequency coil frequency ratio, $\Omega = 0.935$; at zero position, $\lambda = 34$ centimeters; $\dot{B}_z$ probe; bottom of beach at 83 centimeters.

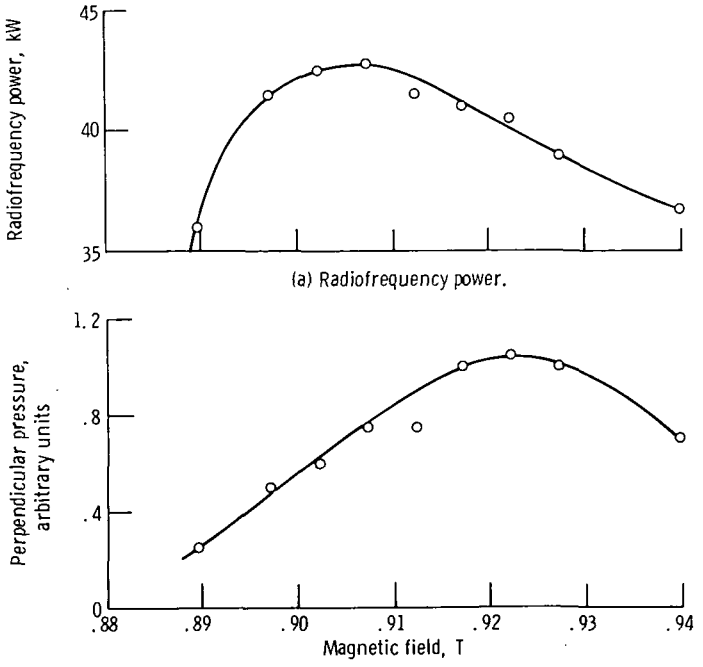

(a) Radiofrequency power.

(b) Perpendicular pressure at beach.

Figure 28. - Effect of magnetic field on radiofrequency power and perpendicular pressure. Radiofrequency current, 250 amperes; gas, deuterium (D_2); full beach.

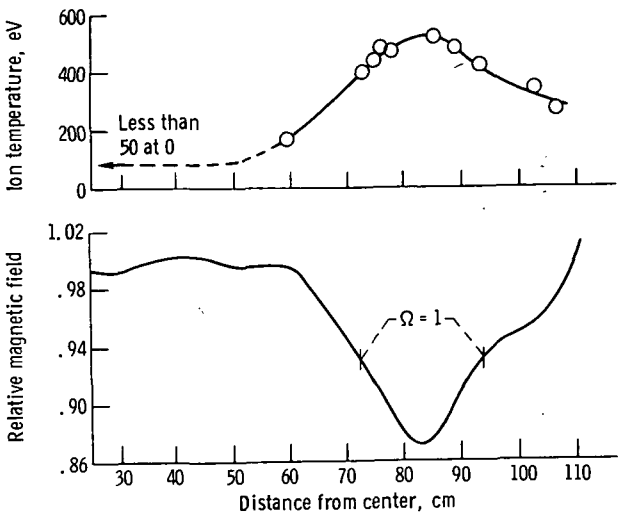

Figure 29. - Axial variation of ion temperature throughout magnetic beach. Frequency ratio, Ω = 0.93 at coil; gas, deuterium (D_2).

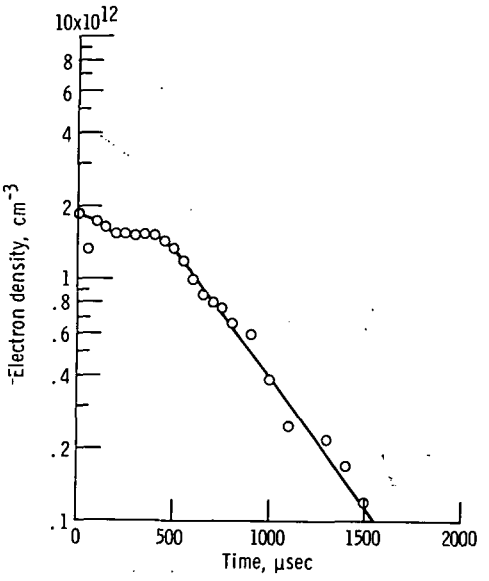

Figure 30. - Typical density as function of time history of plasma.

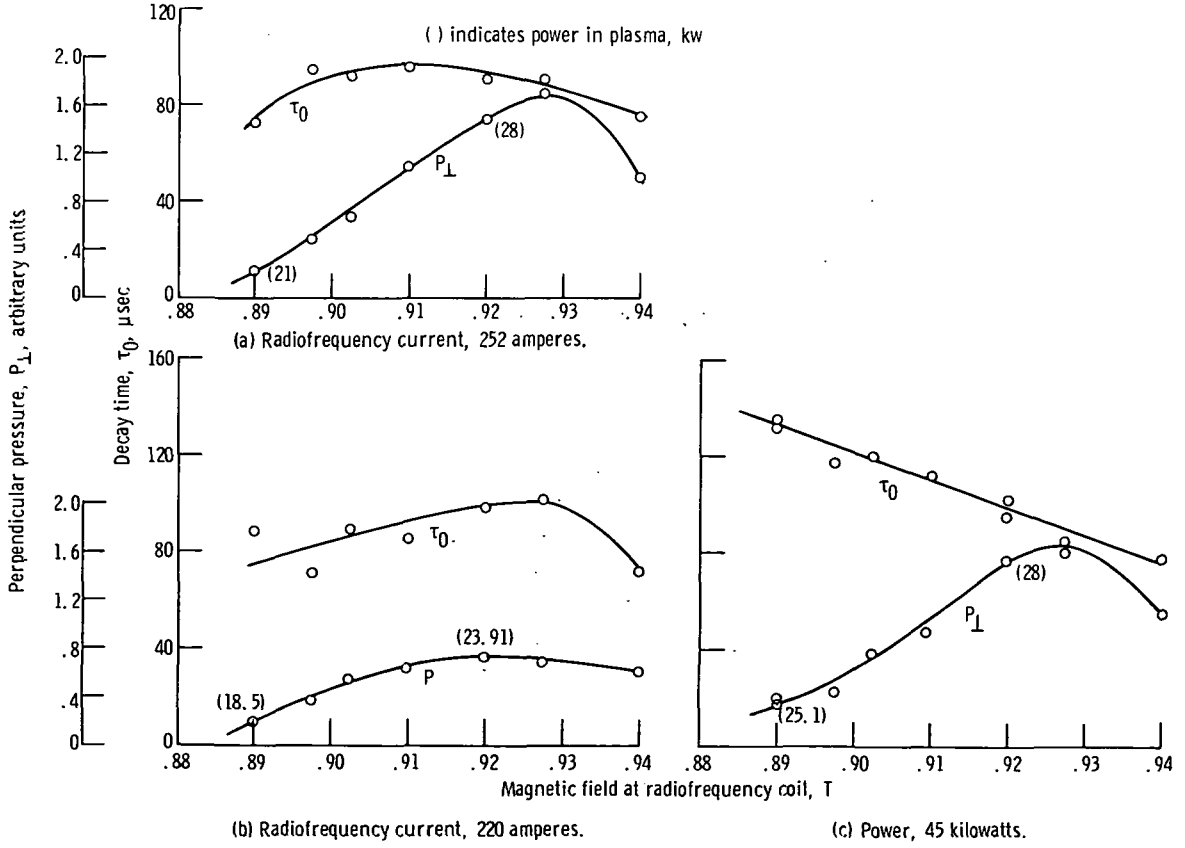

(a) Radiofrequency current, 252 amperes.

(b) Radiofrequency current, 220 amperes.

(c) Power, 45 kilowatts.

Figure 31. - Effect of magnetic field on energy decay time and perpendicular pressure.

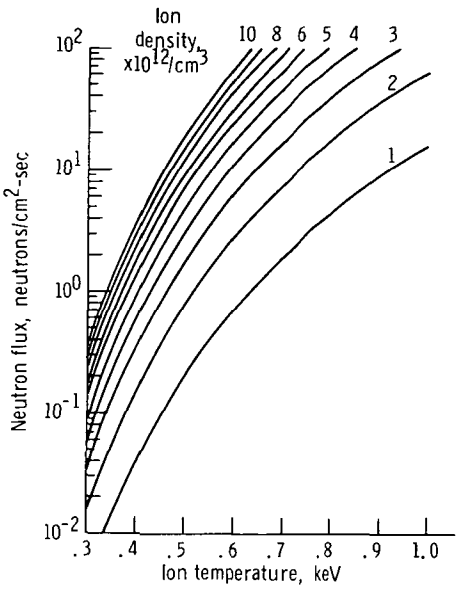

Figure 32. - Calculated neutron flux (50-cm radial distance from magnetic beach).

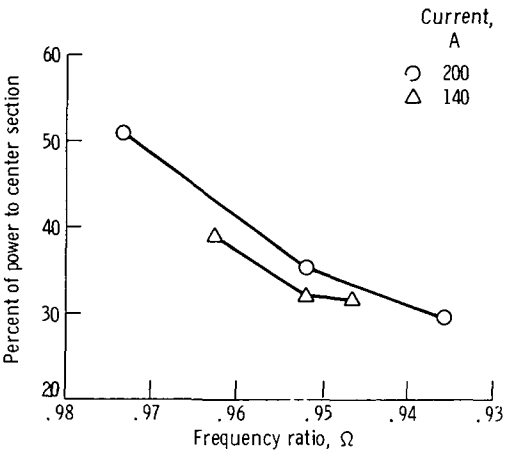

Figure 33. - Power absorbed by center section for two values of radiofrequency current. Gas, hydrogen (H_2).

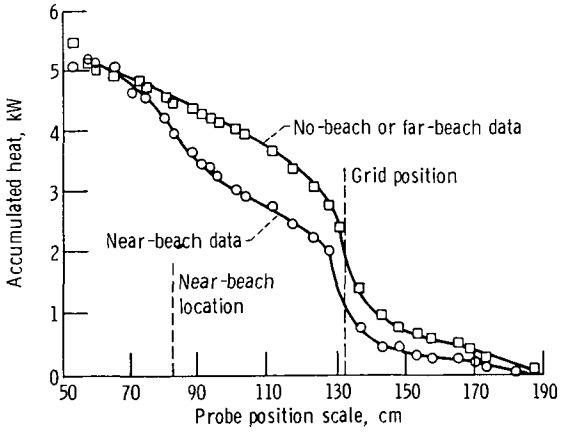

Figure 34. - Heat transfer to arm. Radiofrequency current, 200 amperes; gas, hydrogen (H_2).

NASA-Langley, 1973 — 25 E-7213

NATIONAL AERONAUTICS AND SPACE ADMINISTRATION
WASHINGTON, D.C. 20546

OFFICIAL BUSINESS
PENALTY FOR PRIVATE USE $300

SPECIAL FOURTH-CLASS RATE
BOOK

POSTAGE AND FEES PAID
NATIONAL AERONAUTICS AND
SPACE ADMINISTRATION
451

U.S. MAIL

POSTMASTER: If Undeliverable (Section 158 Postal Manual) Do Not Return

"The aeronautical and space activities of the United States shall be conducted so as to contribute . . . to the expansion of human knowledge of phenomena in the atmosphere and space. The Administration shall provide for the widest practicable and appropriate dissemination of information concerning its activities and the results thereof."

—NATIONAL AERONAUTICS AND SPACE ACT OF 1958

NASA SCIENTIFIC AND TECHNICAL PUBLICATIONS

TECHNICAL REPORTS: Scientific and technical information considered important, complete, and a lasting contribution to existing knowledge.

TECHNICAL NOTES: Information less broad in scope but nevertheless of importance as a contribution to existing knowledge.

TECHNICAL MEMORANDUMS: Information receiving limited distribution because of preliminary data, security classification, or other reasons. Also includes conference proceedings with either limited or unlimited distribution.

CONTRACTOR REPORTS: Scientific and technical information generated under a NASA contract or grant and considered an important contribution to existing knowledge.

TECHNICAL TRANSLATIONS: Information published in a foreign language considered to merit NASA distribution in English.

SPECIAL PUBLICATIONS: Information derived from or of value to NASA activities. Publications include final reports of major projects, monographs, data compilations, handbooks, sourcebooks, and special bibliographies.

TECHNOLOGY UTILIZATION PUBLICATIONS: Information on technology used by NASA that may be of particular interest in commercial and other non-aerospace applications. Publications include Tech Briefs, Technology Utilization Reports and Technology Surveys.

Details on the availability of these publications may be obtained from:

SCIENTIFIC AND TECHNICAL INFORMATION OFFICE

NATIONAL AERONAUTICS AND SPACE ADMINISTRATION

Washington, D.C. 20546